이학박사 학위논문

고지방식이에 의한 대장 섬유아세포 조절 기전 연구

A high-fat diet activates the BAs-FXR axis and triggers cancer-associated fibroblast properties in the colon

울산대학교 대학원

의 과 학 과

김 태 영

A high-fat diet activates the BAs-FXR axis and triggers cancer-associated fibroblast properties in the colon

지 도 교 수　권 미 나

이 논문을 이학박사학위 논문으로 제출함

2023 년 8 월

울산대학교 대학원

의 과 학 과

김 태 영

김태영의 이학박사학위 논문을 인준함

심사위원 김 헌 식 (인)

심사위원 권 미 나 (인)

심사위원 이 희 란 (인)

심사위원 황 성 욱 (인)

심사위원 서 상 욱 (인)

울 산 대 학 교 대 학 원

2023 년 8 월

Abstract

Dietary factors are known to modulate stemness and tumorigenicity of intestinal progenitors. Previous studies demonstrated that high-fat diet (HFD) enhanced numbers of intestinal stem cells (ISCs) and further promoted primary and metastatic colorectal cancer. However, little is known how HFD affects ISC niche which might be involved in initiation of colorectal cancer. Additionally, it is known that HFD can cause dysbiosis in the gut microbiota, resulting in a reduction of diversity and an imbalance in the composition of the gut microbiota. Recent studies have indicated that alterations in gut microbiota induced by HFD can have an impact on intestinal tumorigenesis, but the mechanism underlying the relationship between gut microbiota and colorectal cancer remains unclear. Therefore, understanding the relationship between HFD, ISC niche, and gut microbiota may provide clues for the development of HFD-induced colorectal cancer. In this study, I found that expression of CD44 and Wnt signal-related genes was higher in the colonic crypts of HFD-fed mice than in those fed a purified diet. Within the ISC niche, mesenchymal stromal cells (MSCs) were expanded and secreted predominant levels of Wnt2b in the colon of HFD-fed mice. Of note, increased energy metabolism and cancer-associated fibroblasts (CAFs)-like properties were found in the colonic MSCs of HFD-fed mice. Moreover, colonic MSC from HFD-fed mice promoted the growth of tumorigenic properties and accelerated the expression of cancer stem cells (CSCs)-related markers in colon organoids. In particular, production of deconjugated and secondary bile acids (BAs) was increased through the expansion of bile salt hydrolase-encoding bacteria in HFD-fed mice. Most importantly, BAs-farnesoid X receptor (FXR) interaction stimulated Wnt2b production in colonic CAF-like MSCs. These findings suggest that gut microbiota-mediated BAs-FXR signaling could be a contributing risk factor for HFD-induced colorectal cancer.

Keywords: HFD; CSCs; MSCs, gut microbiota, BAs, FXR

Contents

List of Figures

Introduction

1. Intestinal stem cells and cancer stem cells

The intestinal epithelium is known as the most rapidly self-renewing tissue every four to five days [1]. Intestinal epithelial cells are generated in crypts, migrate rapidly toward the surface, and die at the tip of finger-like protrusions known as villi where cell loss is compensated by constant cell production in crypts. These rapid cellular turnover of the intestine tissue is promoted by leucine-rich-repeat-containing G-protein-coupled receptor 5 (Lgr5) expressing intestinal stem cells (ISCs) existing in the bottom of crypts [2] and Lgr5 acts as a receptor for R-spondins, which are potent Wnt signal enhancers and growth factors of ISCs [3]. ISCs are actively proliferating cells and they give rise to progenitors that can differentiate into the various mature epithelial cells such as enterocytes, goblet cells, enteroendocrine cells, and Paneth cells. The cells with terminal differentiation are generated by amplification of the progenitor pool through several rounds of cell division before differentiation [4]. On the other hands, role of ISCs as cancer-initiating stem cells in the colorectal cancer (CRC) has also been reported [5, 6]. The cancer stem cells (CSCs) are the cells of origin of tumors that are derived from differentiated cells or adult tissue-resident stem cells and they can contribute to tumor malignancies, such as recurrence, metastasis, and heterogeneity [7]. Although evidences were presented regarding various CSC markers and their tumorigenicity [8, 9], there is still lack of experimental evidence as to the factors, which can transform normal ISCs into CSCs.

2. Intestinal stem cell niche

ISC niche not only maintain intestine epithelial homeostasis but also control proliferation and differentiation of ISCs through variety of signaling pathways. The ISC niche is composed of a cellular part and a physical part such as the extracellular matrix (ECM) components. There are Paneth cells and mesenchymal stromal cells (MSCs) in the cellular ISC niche in the small intestine. Paneth cells are located between ISCs and progenitor parts in intestinal crypt region and known to supply Wnt3, epidermal growth factor (EGF), and Notch ligands [10]. MSCs, as connective tissue cells, secrete indispensable signaling molecules and growth factors to maintain ISC homeostasis [11-13]. In case of colon which does not possess Paneth cells, deep crypt secretory (DCS) cells are proposed as one of ISC niche [10, 14]. As like as Paneth cells in the small intestine, $Reg4^+$ DCS cells in the colon are intermingled with colonic stem cells at bottom of crypt regions by providing EGF and Notch ligands [14]. Of interest, DCS cells do not produce the Wnt ligands, whereas Paneth cells produce high levels of Wnt3 [14]. Nonetheless, colonic stem cells express Wnt receptors because colonic MSCs surrounding crypts provide Wnt ligands (i.e., Wnt2b, Wnt4 and Wnt5a) [11, 14].

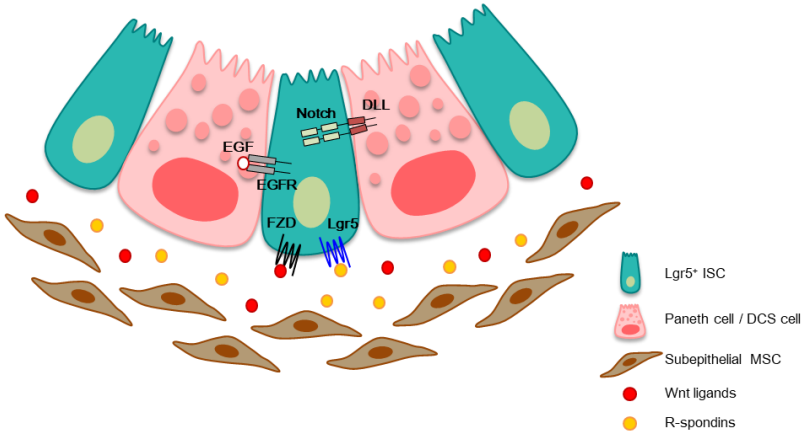

Figure 1. Intestinal stem cell niche in the colon. Lgr5 intestinal stem cells (ISCs) were supported through signaling molecules provided by their niche. $Reg4^+c\text{-}Kit^+$ deep crypt secretory (DCS) cells provide epidermal growth factor (EGF) and Notch ligand, while mesenchymal stromal cells (MSC) secrete Wnt ligand and R-spondin to maintain the stemness of ISCs in colon.

3. Intestinal mesenchymal stromal cells

The intestinal MSCs are composed of various cell types such as stromal cells (telocytes), fibroblasts, and smooth muscle cells [15, 16]. Subepithelial MSCs are located within the lamina propria in close proximity to the ISCs and crypt–villus junction. MSCs are known to provide signaling molecules such as Wnt ligands and R-spondins in the stromal niche for ISCs maintenance [11-13] and improve intestinal epithelial repair by injury [17, 18]. Recent study suggested that FOXL1-expressing MSCs are an important source of producing Wnt ligands [16] and GL1-expressing subepithelial MSCs are an essential ISC niche providing Wnt ligands [19]. Although MSCs support maintenance of ISCs, they have duplicity in that they contribute to cancer development [20]. Cancer-associated fibroblasts in tumor microenvironment promote tumor development and progression through secretion of cytokines, growth factors, and ECM. I therefore speculate that MSCs play an indispensable role to control colonic stem cells and CSCs.

4. Wnt signaling pathway

During the process of Wnt secretion, all Wnt proteins undergo lipid modification in which palmitate is attached by the palmitoyltransferase, Porcupine, which resides in the endoplasmic reticulum (ER) [21]. Thereafter, the transmembrane protein Wntless (Wls) binds only lipid-modified Wnt proteins and transports them to the plasma membrane to secrete. When the secreted Wnt ligands arrive at the target cells, Wnt ligands bind to their cognate Frizzled receptors through their palmitic acid group. Wnt ligands then bind to the low-density-lipoprotein related receptor 5 and 6 (LRP5/6) co-receptor and form a complex with Frizzled, and mediate signal transduction by translocation of β-catenin to nuclear [21]. Wnt signaling is essential for both stem cell maintenance and tissue regeneration; however, ectopic Wnt signaling causes variety of cancers and promotes tumor progression [22]. In particular, ectopic Wnt signaling in the ISCs promote the progression of intestinal tumors [5]. Importantly, it was demonstrated that the Wnt ligands produced by Paneth cells or fibroblasts can influence the initiation and progression of cancer through paracrine fashion [23, 24].

5. HFD and intestinal stem cells

Previous studies have demonstrated that ISCs are influenced by dietary factors and can remodel the composition of the intestinal epithelium [25-27]. Self-renewal and differentiation of ISCs can be regulated through cell-autonomous and non-autonomous mechanisms in response to dietary factors. Calorie restriction enhances the function of ISCs by affecting neighboring Paneth cells through non-autonomous mechanisms [27]. As an example of a cell-autonomous mechanism, the ketogenic diet increases stemness by controlling β-hydroxybutyrate production in ISCs [28]. Dietary L-glutamate also enhances the proliferation of ISCs through the increase of cytosolic Ca^{2+} concentration [29]. Especially, HFD directly enhanced the numbers and functions of $Lgr5^{+}$ ISCs through the peroxisome proliferator activated receptor-delta (PPAR-δ) signaling, which is activated by fatty acids [30]. Of note, activated PPAR-δ signaling from HFD amplifies canonical Wnt signaling in ISCs and progenitor cells, and in vivo PPAR-δ agonist treatment increase the capability to initiate tumors from intestinal progenitor cells [30]. Although it has been suggested that dietary fat play a role in regulating the function of the ISC, the mechanisms and interactions between HFD and the various ISC niche cells are still unclear.

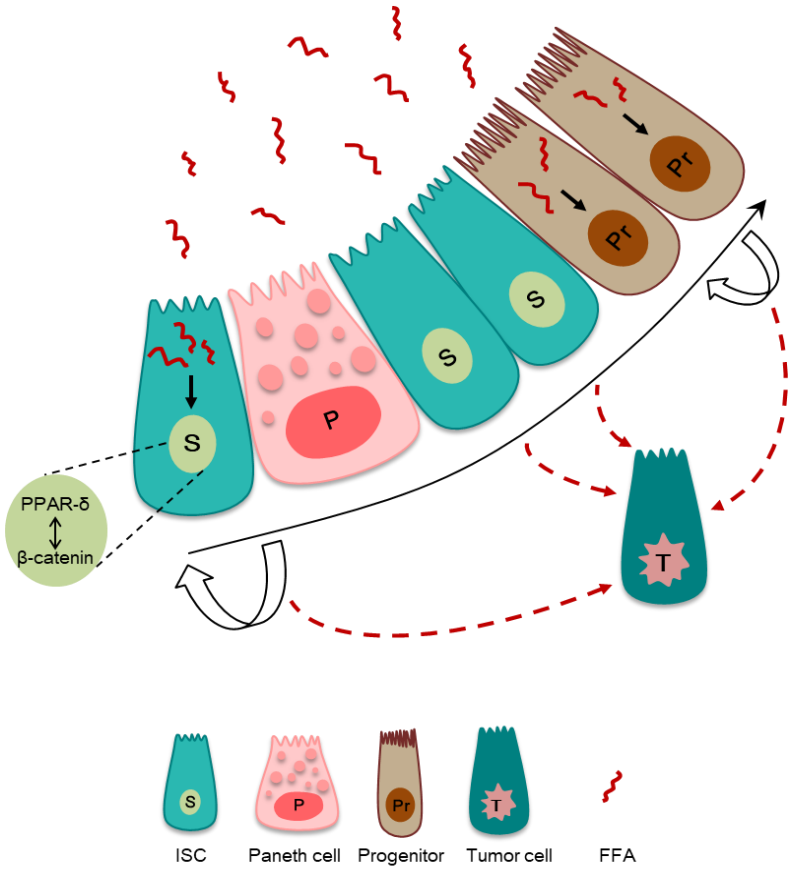

Figure 2. Intestinal tumorigenesis increased by HFD. In the intestine, FFA increased by HFD promotes binding to nuclear PPAR-δ in ISCs and progenitors. PPAR-δ signaling activated by FFA binding stimulates β-catenin target genes by β-catenin translocation to the nucleus. Activated β-catenin target genes increase the numbers and function of ISCs. Notably, HFD confers regenerative capacity on progenitors and trigger the conversion of ISCs as well as progenitors into tumor cell.

6. Diet and gut microbiota

The commensal gut microbiota provides beneficial effects to host and reside within the mucosal layer of the digestive tract of host. The human gastrointestinal tract harbors over 100 trillion gut microbiota, with the colon containing the most diverse and abundant microbial community among all the tissues [31]. It is well established that the dominant gut microbial phyla in healthy humans are *Firmicutes*, *Bacteroidetes*, *Actinobacteria*, *Verrucomicrobia*, and *Proteobacteria* [32]. The composition of the gut microbiota can be influenced by various lifestyle factors, and among them, dietary factors are known to have a close relationship with the gut microbiota [33]. Changes in the composition of the gut microbiota can result in dysbiosis, which causes an imbalance between beneficial and potentially pathogenic bacteria in the gut [34]. This imbalance can lead to the development of chronic inflammatory disease, such as inflammation, metabolic disorder, and cancer [34].

It is known that HFD disrupts the balance of gut microbiota, increasing *Firmicutes* and *Proteobacteria* while decreasing *Bacteroidetes* [35]. HFD can lead to low-grade chronic intestinal inflammation, which is closely related to the gut microbiota [36, 37]. In previous study, it was observed that HFD induced production of TNF-α in intestine of specific-pathogen free mice but not in germ-free mice [38]. Constant consumption of a HFD induces the expansion of pathobiont *E. coli* in the colon, thereby inducing dysfunction of the colonic epithelial layer, reduced production of mucus and anti-microbial proteins, and ultimately an inflammation [39, 40]. Conversely, certain gut microbiota such as *Lactobacillus* and *Faecalibacterium*, which can induce the anti-inflammatory response, are known to decrease under HFD consumption [41-43]. The gut microbiota-derived molecules and metabolites play an important role in regulating the host's immune response. One of the short-chain fatty acids (SCFAs), butyrate, contributes to maintaining intestinal homeostasis by promoting the activation of cytotoxic $CD8^+$ T cells or differentiation of regulatory T cells in the intestine [44, 45]. The consumption of HFD is recognized to decrease the production of these beneficial SCFAs owing to a lack of dietary fiber [46]. Additionally, recent studies have suggested that alteration of gut microbiota by HFD is closely associated with the development of intestinal tumorigenesis independently of obesity [47, 48]. However, there is still a lack of evidence on the

mechanisms by which dysbiosis of the gut caused by a HFD promotes the development of CRC.

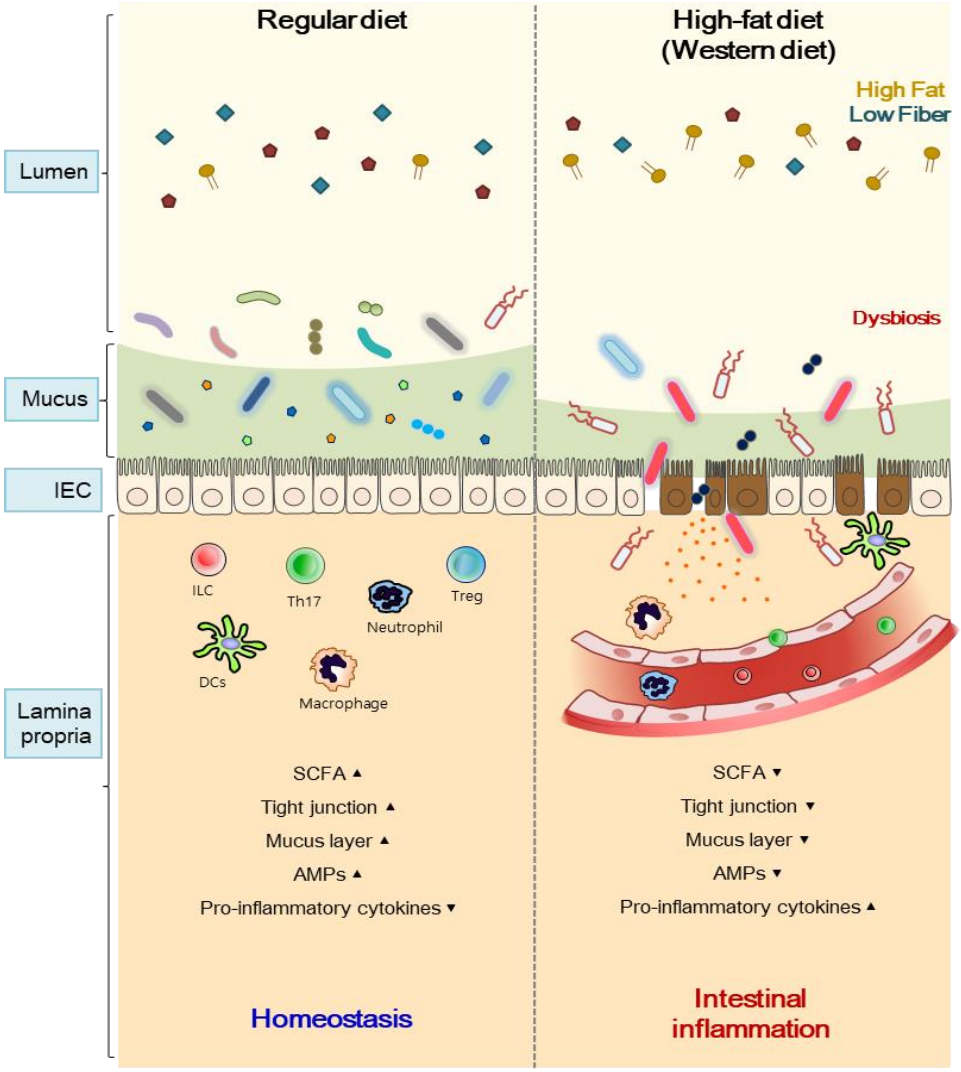

Figure 3. The role of dietary factors and gut microbiota in intestinal homeostasis. High-fat and lack of fiber cause an imbalance in gut microbiota composition, resulting in a decrease in beneficial bacteria and an increase in pathogenic bacteria. These gut microbial dysbiosis can lead to diminished production of microbial short-chain fatty acids (SCFAs), decreased expression of tight junction and mucin, and impaired production of anti-microbial peptides. As a consequence, HFD-induced dysbiosis disrupt the intestinal epithelial barrier and increase bacterial translocation, leading to a recruitment of inflammatory cells and upregulation of pro-inflammatory cytokines, ultimately resulting in intestinal inflammation.

7. Bile acid metabolism

Bile acids (BAs) are produced in the liver by the enzyme cholesterol 7α-hydroxylase (CYP7A1) or from cholesterol, and then secreted into the intestine to aid in the absorption of lipids [49]. The synthesis of bile acids can be regulated by a negative feedback loop involving CYP7A1, which is activated by the farnesoid X receptor (FXR) in both the liver and intestine [50]. Before being released into the duodenum, primary BAs are conjugated with amino acids glycine or taurine to form sodium salts, which improves their solubility [49]. After a meal, the secretion of cholecystokinin in the intestine triggers gallbladder contraction, which results in the release of bile acids into the intestine [49]. BAs can be reabsorbed in the ileum through sodium-dependent transporter (ASBT) of enterocytes and recycled to the liver via the hepatic portal vein, preserving more than 95% of the BA pool [51]. Small amounts of primary BAs are capable of escaping the process of enterohepatic reabsorption and becoming deconjugated by the bile salt hydrolase (BSH), which is produced by gut microbiota [52]. Gut microbiota in the colon convert deconjugated BAs into secondary BAs through enzymatic reactions, including dehydrogenation, dehydroxylation, and epimerization, and promote their passive reabsorption [52]. Previous study suggested that disturbance of gut microbiota can affect the BA pool size and composition [53]. A recent study showed that changes in BA metabolism by bacteria were linked to various inflammatory autoimmune disorders, including inflammatory bowel disease and type 1 diabetes [54]. Given that gut microbiota can modulate the BA metabolism, the interaction between diet, gut microbiome, and bile acid metabolism may be a clue to the development of CRC by HFD. It has also been shown that activation of BA-responsive receptors such as FXR and G-protein coupled receptor TGR5 regulates the maintenance of ISC and epithelial regeneration [55-57]. However, despite the established role of gut microbiota-derived BAs in ISC function and maintenance, the underlying mechanism of BAs on the regulation of the ISC niche remains undetermined.

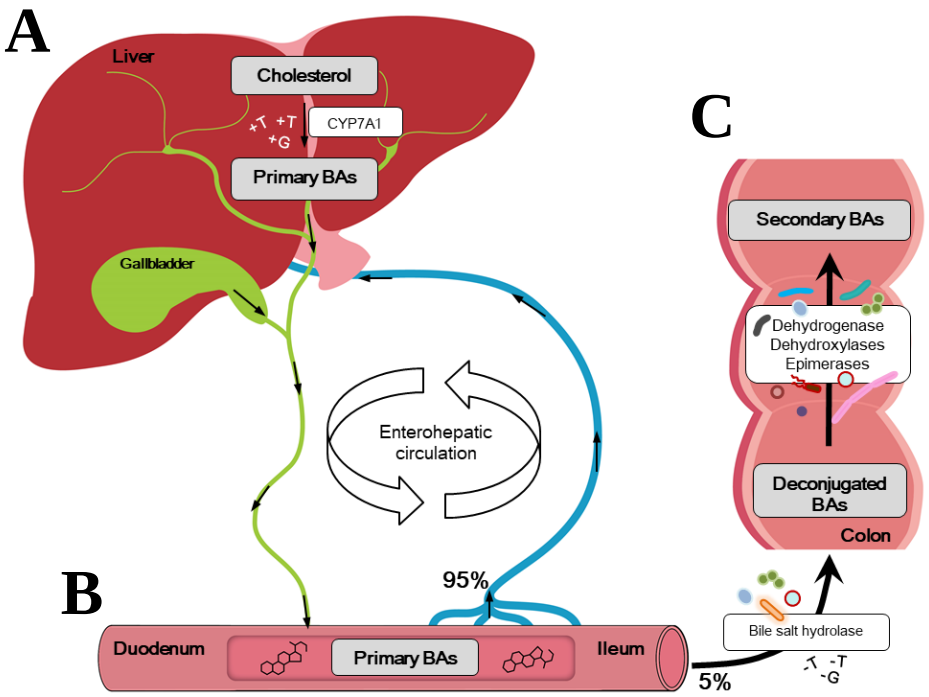

Figure 4. Classic bile acid metabolism. (A) Primary bile acids (BAs) are synthesized by cholesterol 7α-hydroxylase (CYP7A1) in the liver. Primary bile BAs are conjugated with glycine or taurine, and they are stored in the gallbladder. (B) Primary BAs are released into the duodenum, and around 95% of them undergo enterohepatic circulation to be recycled before reaching the ileum. (C) The remaining 5% of BAs pool undergoes modification through enzymatic reactions that are derived from gut microbiota, starting from the ileum and continuing to the colon. Deconjugated BAs in the ileum are transformed into secondary BAs in the colon through various enzymatic reactions such as dehydrogenase, dehydroxylase, and epimerase.

8. The rationale of my study

HFD is known to alter the ISC properties and modulate the tumorigenicity of intestinal progenitor cells; however, the impact of a HFD on the ISC niche and its association with CRC remains unclear. In this study, I addressed the potential role of colonic MSCs on development of HFD-induced CRC. My findings demonstrated HFD-induced CAF-like MSCs play an indispensable role in balancing the properties of CSCs through activation of the BAs-FXR axis.

Materials and Methods

Mice and diet

C57BL/6N mice were purchased from Orient Bio (South Korea), and *Lgr5-EGFP-IRES-CreERT2* mice and C57BL/6J-*Apc*$^{Min/+}$ mice were purchased from Jackson Laboratory (Bar Harbor, ME). All mice were housed under specific pathogen-free conditions in the animal facility at Asan Medical Center, where they received water *ad libitum*. Three different types of diets were used throughout the experiment; standard normal chow diet (NCD; Purina 5057, Purina), purified diet (PD; D10012G, Research Diets), and 60% kcal HFD (D12492, Research Diets). Mice received their respective food *ad libitum* from the age of 6 weeks and until at least 2 months. Mice were sex- and age-matched between groups. *Apc*$^{Min/+}$ mice with spontaneous intestinal adenoma after housing for 15 weeks were used for colon cancer organoids culture.

Experimental inflammation-induced colorectal cancer model

Mice were given a single intraperitoneal injection of AOM (10 mg/kg body weight, Sigma Aldrich) combined with three cycles of DSS treatment as illustrated in Figure 7A.

Histology

Intestines were rolled using the Swiss roll technique and fixed in 4% paraformaldehyde (PFA). They were then dehydrated through a chain of graded ethanol baths and embedded in paraffin. The paraffin-embedded blocks were cut into 5 μm sections and stained with hematoxylin and eosin (H&E) or periodic acid Schiff (PAS). For the PAS staining, tissue section-slides were deparaffinized and rehydrated and placed in 1% periodic acid solution at RT for 5 min. Slides were then washed and immersed in Schiff's reagent for 15 min and stained with hematoxylin.

Histological scoring

Histological grade was scored by blinded investigators through a scoring system as described previously [58]: the severity of inflammation (0, none; 1, slight; 2, moderate; 3, severe), the extent of injury (0, none; 1, mucosa; 2, mucosa and submucosa; 3, transmural and epithelium lost), and crypt damage (0, none; 1,basal one-third damaged; 2, basal two-thirds damaged; 3, only surface epithelium intact; 4, entire crypt and epithelium lost). Finally, the percentage of involvement by the disease conditions was quantified in these indicators (0, 0–25%; 1, 26–50%, 2, 51–75%; 3, 76–100%).

Immunofluorescence staining

Intestines were prepared by the Swiss roll technique for the frozen section and fixed in 4 % paraformaldehyde (PFA). Tissues were then dehydrated stepwise with 15 % and 30 % sucrose in PBS. Thereafter, rolled tissues were embedded in optimal cutting temperature compound (Sakura Finetek), frozen, sliced to 5 μm, and tissue sections were fixed in −20℃ acetone for 5 min. Paraffin or cryosections were permeabilized in PBS containing 0.5 % Triton X-100 at RT for 20 min and blocked with 5 % BSA in PBS at RT for 1hr. Tissue sections were then stained with primary antibodies overnight at 4℃. After washing with PBS, tissue sections were incubated with secondary antibodies at RT for 1 hr, stained with 4′, 6-diamidino-2-phenylindole (DAPI; Thermo Fisher) for 2 min at RT, and mounted with PermaFluor mountant (Thermo Fisher). To analyze the immunofluorescence of intestinal MSCs, plated MSCs were fixed with 4 % PFA in PBS. After MSCs were washed in PBS, cells were permeabilized in PBS containing 0.5 % Triton X-100 at RT for 30 min. After staining, fluorescent images of all samples were captured on an LSM 710 confocal microscope (Carl Zeiss). The following antibodies were used for staining: anti-Ki67 (BioLegend, clone 11F6), anti-CD44s-v (Abcam, IM7) anti-β-catenin (BD Biosciences, clone 14), anti-gp38 (R&D), anti-CD90 (Abcam, IBL-6/23), and anti-Wnt2b (Abcam, clone EPR13386), Alexa fluor 546-conjugated donkey anti-rat IgG (Thermo Fisher), Alexa fluor

488-conjugated goat anti-mouse IgG (Abcam), Alexa fluor 488-conjugated donkey anti-rat IgG (Lifetechnologies), and Alexa fluor 647-conjugated donkey anti-goat IgG (Abcam).

RNA in situ hybridization

According to the manufacturer's instructions, the intestines were fixed in 4% PFA, embedded in paraffin, and used for RNA in situ hybridization (RNAscope 2.5 HD Detection kit, Advanced Cell Diagnostics). *Axin2*, *Wnt2b*, *Wnt2*, *Wnt3*, *Wnt4*, *Wnt5a*, *Wnt6*, and *Wnt9b* probes were purchased from Advanced Cell Diagnostics and hybridized to their target mRNA.

Crypt isolation

Fat and adherent connective tissues were removed to obtain crypts from the colon. Colon tissues were then opened longitudinally, washed with cold PBS without magnesium chloride and calcium by vigorously shaking, and cut into approximately 1 cm sections. Tissue pieces were incubated in PBS containing 5 mM EDTA/gentamicin (Gibco) at 37℃ for 30 min. Tissue pieces were washed with PBS, vigorously shaken, and then filtered by a 70 μm cell strainer (BD Falcon) to isolate the intestinal crypts.

Organoids culture and measurement

Colonic crypts were pelleted and resuspended with TrypLE Express (Thermo Fisher) for 15 min at 37℃ to dissociate crypts as described previously [59]. Dissociated colonic crypts were counted by a hemocytometer and embedded (2×10^4 cells / well) in Matrigel (Corning). Matrigel containing crypts was plated at 50 μL per well onto a flat-bottom 24-well plate (Thermo Fisher) and cultured in WENR medium containing B27 supplement (Thermo Fisher), N2 supplement (Thermo Fisher), N-acetyl cysteine (Sigma Aldrich), EGF (Thermo Fisher), Noggin (R&D Systems), Wnt3a-conditioned medium, R-spondin-1-conditioned

medium, Antibiotic-Antimycotic (Thermo Fisher), HEPES (Gibco), GlutaMAX (Gibco), and advanced DMEM/F12 (Thermo Fisher). Y-27632 (Sigma Aldrich) and Jagged-1 (AnaSpec) were added to WENR medium for 3 days after the start of the culture, as described previously [60]. To manipulate the cancer organoids, colonic crypts from *Apc*$^{Min/+}$ mice were isolated and cultured in EN medium without Wnt3a and R-spondin-1. The culture medium was changed every 2 to 3 days. Organoids were mechanically disrupted by pipetting for subculture or further incubated in TrypLE Express Enzyme at 37℃ for 15 min. Organoids were randomly photographed using an inverted microscope (Carl Zeiss), and each photo was analyzed using ImageJ software (NIH) to measure the surface area. The perimeters for area measurements were defined manually by automated ImageJ software.

Treatment of fatty acids and cecal microbial products

The following fatty acids have been applied to both organoids and MSCs: palmitic acid (30 μM; Sigma Aldrich), oleic acid (30 μM; Sigma Aldrich), stearic acid (30 μM; Sigma Aldrich), or lipid mixture (1%; Sigma Aldrich). All fatty acids were conjugated with BSA. For CMP, cecal contents were lyophilized, and the powder was dissolved in the advanced DMEM/F12 medium and vigorously vortexed for 1 hr at 4 ℃. After centrifugation, the supernatant was filtered using a 0.2 μm syringe filter (PALL) and treated into MSCs with titration.

MSCs culture

Colonic MSCs were isolated as described previously [61]. In brief, the remaining colon tissues after crypt isolation were chopped and added with DMEM medium (Gibco) containing 10% heat-inactivated FBS (Gibco), gentamycin/streptomycin, and collagenase type IV (Sigma Aldrich), and incubated for 1 hr at 37℃ with shaking (200 rpm). Dissociated tissues were shaken vigorously and supernatants were passed through a 70 μm cell strainer (BD Falcon). Cell pellets were collected by centrifuge at 280 × g for 10 min, washed, and cultured in advanced DMEM/F12 medium containing 10% FBS (Gibco), 2 mM GlutaMax (Gibco), 1%

Penicillin–Streptomycin (Thermo Fisher), and, 1% Antibiotic-Antimycotic (Thermo Fisher). MSCs were sub-cultured to obtain high purity cells.

Flow cytometry

Isolated MSCs were blocked with solution containing 0.2% BSA in PBS and stained with Live/Dead cell stain kit (Thermo Fisher) and antibodies; anti-CD45 (BD Biosciences, clone 30-F11), anti-CD31 (BD Biosciences, clone MEC13.3), anti-EPCAM (eBioscience, clone G8.8), anti-gp38 (BioLegend, clone 8.1.1), and anti-CD90 (eBioscience, clone 53-2.1). Flow cytometry was performed using a FACS CANTO II (BD Biosciences) and files were analyzed using FlowJo software (Tree Star).

Co-culture with organoids and MSCs

MSCs (2×10^4 / well) were suspended in Matrigel matrix in the presence of organoids (2×10^4 / well) obtained from NCD-fed control mice or *Apc*$^{Min/+}$ mice. After the Matrigel polymerization, cells were cultured in ENR medium (without Wnt3a) or EN medium. C59 (10μM; Abcam) was treated in ENR medium at 7 days post culture to inhibit Wnt secretion.

Real time-qPCR

Total RNA was extracted using the RNeasy mini kit (QIAGEN). RNA was converted to cDNA with Superscript II reverse transcriptase and oligo (dT) primer (Thermo Fisher). cDNA was used as the template for real-time qPCR performed using SYBR green chemistry (Affymetrix) on an ABI 7500 Real-Time qPCR System (Applied Biosystems). The primer sequences used for real-time qPCR are as follows: *Lgr5*, Fw 5'-CCTGTCCAGGCTTTCAGAAG-3', Rev 5'-CTGTGGAGTCCATCAAAGCA-3'; *CD44*, Fw 5'-TCCTTCTTTATCCGGAGCAC-3', Rev 5'-ACGTCTCCTGCTGGGTAGC- 3'; *Reg4*, Fw 5'-CTGGAATCCCAGGACAAAGAGTG-3', Rev 5'-CTGGAGGCCTCCTC

AATGTTTGC-3'; *c-Kit*, Fw 5'-TCATCGAGTGTGATGGGAAA-3', Rev 5'-GGTGACT TGTTTCAGGCACA-3'; *Egf*, Fw 5'-TTCTCACAAGGAAAGAGCATCTC-3', Rev 5'-GTCCTGTCCCGTTAAGGAAAAC-3'; *Egfr*, Fw 5'-GCTGGTGTTGCTGACCGCG-3', Rev 5'-GGGTGAGCCTGTTACTTGTGCC-3'; *ErbB2*, Fw 5'-GCAAGCACTGTCTGCCA TGC-3', Rev 5'-GGGCACAAGCCTCACACTGG-3'; *Notch1*, Fw 5'-GCTGCCTCTTTGA TGGCTTC-3', Rev 5'-CACATTCGGCACTGTTACAG-3'; *Dll1*, Fw 5'-CAGGACCTTC TTTCGCGTAT-3', Rev 5'-AAGGGGAATCGGATGGGGTT-3'; *Dll4*, Fw 5' TTCCAGG CAACCTTCTCCGA-3', Rev 5'-ACTGCCGCTATTCTTGTCCC-3'; *Hes1*, Fw 5'-CCAGC CAGTGTCAACACGA-3', Rev 5'-AATGCCGGGAGCTACTTTC-3'; *Fzd5*, Fw 5'-CCGC ATACCACAAGCAAG-3', Rev 5'-GCATCAGCACCAAGAAGG-3'; *Ctnnb1*, Fw 5'-AT GGAGCCGGACAGAAAAGC-3', Rev 5'-TGGGAGGTGTCAACATCTTC-3'; *Axin2,* Fw 5'-AACCTATGCCCGTTTCCTCT-3', Rev 5'-GAGTGTAAAGACTTGG TCCA-3'; *Gsk3β,* Fw 5'-ACCGACAACCACCTCCTTTG-3', Rev 5'-TCACAGGGAGTGTCTGCTT G-3'; *Cyclin D1*, Fw 5'-GCGTACCCTGACACCAATCTC- 3', Rev 5'-CTCCTCTTCGCA CTTCTGCTC-3'; *c-Myc*, Fw 5'-TGAGCCCCTAGTGCTGCAT-3', Rev 5'-AGCCCGAC TCCGACCTCTT-3'; *Lef*, Fw 5'-TGTTTATCCCATCACGGGTGG-3', Rev 5'-CATGGA AGTGTCGCCTGACAG-3'; *Apc*, Fw 5'-AGCCATGCCAACAAAGTCATCACG-3', Rev 5'-TTCCTTGCCACAGGTGGAGGTA-3'. *Epcam,* Fw 5'-ATGGACCTGAGAGTGAAC GG-3', Rev 5'-CACGGCTAGGCATTAAGCTC-3'; *CD24*, Fw 5'-GTTGCACCGTTTCCC GGTAA-3', Rev 5'-CCCCTCTGGTGGTAGCGTTA-3'; *CD166*, Fw 5'-ATGGCATC TAAGGTGTCCCCT-3', Rev 5'-CTGAGTTGACAGTGTACCATCC-3'; *CD29*, Fw 5'-ATGCCAAATCTTGCGGAGAAT-3', Rev 5'-TTTGCTGCGATTGGTGACATT-3'; *Aldh1a1,* Fw 5'-ATACTTGTCGGATTTAGGAGGCT-3', Rev 5'-GGGCCTATCTTCC AAATGAACA-3'; *Ephb2*, Fw 5'-TCATCGCTGTGGTCGTCATTG-3', Rev 5'-GTCC GCTGGTGTAGTGTTGTAG-3'; *Wnt2b,* Fw 5'-CCGTGTAGACACGTCCTGGT-3', Rev 5'-TGATGTCTGGGTAGCGTTGA-3'.

RNA-seq analysis

Total RNA was extracted using the RNeasy mini kit (QIAGEN). A library was prepared with 1μg of total RNA for each sample using the TruSeq Stranded mRNA LT Sample Prep kit (Illumina). The protocol was performed with polyA-selected RNA extraction, RNA fragmentation, random hexamer-primed reverse transcription, and 101 nt paired-end sequencing by the NovaSeq6000 platform (Illumina). The libraries were quantified using qPCR according to the qPCR Quantification Protocol Guide (KAPA Library Quantification Kit for Illumina Sequencing platforms) and qualified using the 2100 Bioanalyzer (Agilent Technologies). RNA-seq experiments and statistical analyses were performed by Macrogen Inc (Seoul, South Korea). The reads were pre-processed to remove low-quality and adapter sequences before analysis, and processed reads were aligned to *Mus musculus (mm10)* using HISAT v2.0.5. After alignment, raw data were obtained through the StringTie v1.3.3b to assemble aligned reads into transcripts and estimate their abundance. Filtered data were $\log_2$-transformed and subjected to quantile normalization. For pathway analysis, significant gene lists were performed based on the KEGG pathway. For GSEA, the raw gene matrices count was normalized and performed with GSEA software using a pre-ranked dataset. *P* values in the GSEA data were estimated by 1000 permutations.

16s rRNA sequencing for metagenomic analysis

Bacterial DNA was extracted from feces using QIAamp DNA stool mini kits (QIAGEN). PCR amplification was performed using primers targeting the segment from the V3 to V4 regions of the 16S rRNA gene with extracted DNA. For bacterial amplifications, I used barcoded primers of 341F (5′-CCTACGGGNBGCASCAG-3′) and 805R (5′-GACTACNVGGGTATCTAATCC-3′). The amplifications were performed under the following conditions: initial denaturation at 95 ℃ for 5 min, followed by 30 cycles of denaturation at 95 ℃ for 30 sec, primer annealing at 55 ℃ for 30 sec, and extension at 72 ℃ for 30 sec, with final elongation at 72 ℃ for 5 min. The QIAquick PCR purification kit (Qiagen) was used to purify the purification of the amplified products. Equal concentrations

of purified products were pooled, and short fragments (non-target products) were removed with an AMPure bead kit (Agencourt). The quality and product size were assessed on a Bioanalyzer 2100 (Agilent) using a DNA 7500 chip. Mixed amplicon sequencing was conducted by emulsion PCR and then deposited on picotiter plates. The sequencing was carried out at Chunlab (Seoul, South Korea) on a GS Junior Sequencing System (Roche) per the manufacturer's instructions. Taxonomic cladogram was analyzed using LEfSe with a threshold 2 on the logarithmic LDA score [62].

Measurement of OCR and ECAR by XF24 Flux Analyzer

Primary cultured colonic MSCs were seeded at 4×10^4 cells per well in XF24 cell culture microplates (Agilent Technologies) and cultured in MSC culture media overnight. One hr before measurement, culture media was replaced with OCR assay media [minimal DMEM (Sigma Aldrich) and supplemented with 20 mM glucose (Junsei Chemical), 2 mM GlutaMax (Gibco), and 5 mM pyruvate (Sigma Aldrich)] or ECAR assay media (minimal DMEM and supplemented with 2 mM GlutaMax) in the 37℃ non-CO_2 incubator. The Seahorse Bioscience XF24 analyzer (Agilent Technologies) was used to measure OCR and ECAR. For OCR measurements, 1 μM oligomycin (Sigma Aldrich), 1 μM FCCP (Sigma Aldrich), and 1 μM rotenone and antimycin (Sigma Aldrich) were injected. For ECAR measurements, 10 mM glucose, 2 μM oligomycin, and 50 mM 2-deoxy-D-glucose (Sigma Aldrich) were injected. The parameters of glycolytic function, glycolytic capacity, glycolytic reserve, and non-glycolytic acidification were calculated using Seahorse Wave software V2.6.

Analysis of free fatty acids using GC-MS/MS

The CMP was lyophilized by Freeze Dryer (CHRIST) after pre-freezing overnight at –80℃. The powder was homogenized with cold methanol (MeOH) and internal standard solution (0.1 mg / mL myristic acid-d_{27}). Sample solutions were acidified with HCl to 25 mM final concentration and centrifuged. Supernatants were collected into fresh tubes, and iso-octane

was added. The upper phase was collected after the liquid–liquid extraction process and dried under vacuum. The dried sample was combined with BCl_3-MeOH, 12% (w/w, Sigma Aldrich) at 60℃ for 30 min. H_2O and hexane were added sequentially, and the sample was mixed vigorously. The upper phase was collected after resting the sample for 5 min. Anhydrous sodium sulfate was added, and the supernatant was then ready for GC/MS analysis. Fatty acid methyl esters (Sigma Aldrich) were used to generate calibration curves without derivatization and analyzed with the GC-MS system (Agilent 7890A/5975C) using capillary columns (HP-5MS, 30 m × 0.25 mm × 0.2 μm). Electron impact (EI) ionization was used in positive ion mode. One μL of injection volume and split mode (ratio 10:1) were used. Extracted ion chromatogram by the specific fragment ion per fatty acid was used to quantify the negative ion mode. Data analysis was performed using MSD ChemStation software (Agilent E02.02.1431).

Analysis of SCFA using GC-MS/MS

The CMP was lyophilized by Freeze Dryer (CHRIST) after pre-freezing overnight at –80℃. Ten mg of freeze-dried feces was homogenized vigorously with 400 μL of internal standard solution [1 mM propionic acid (C3)-d6 and 100 μM butyric acid (C4)-d7] in water. After centrifuging, the supernatant was filtered out. AABD-SH (20 μL of 20 mM), TPP (20 μL of 20 mM), and DPDS (20 μL) in dichloromethane were added to the filtrate. The solution was incubated for 10 min at RT with vortexing and dried under vacuum. The sample was reconstituted with 80 μL of methanol prior to LC-MS/MS analysis. The LC-MS/MS system was equipped with a 1290 HPLC (Agilent Technologies, Denmark), Qtrap 5500 (ABSciex), and a reverse-phase column (Pursuit 5 C18 150 × 2.0 mm; Agilent Technologies). The extracted ion chromatogram (EIC) corresponding to a specific transition for each metabolite was used for quantitation. The area under the curve of each EIC was normalized to the EIC of the internal standard. The peak area ratio of each metabolite was normalized to the internal standard using serum volume or tissue weight in a sample, and then used for relative comparison.

Analysis of BAs using LC-MS / MS

Feces were collected through individual housing for 1 day and lyophilized by Freeze Dryer (CHRIST) after pre-freezing overnight at –80℃. Ten mg of freeze-dried feces was homogenized with 50% MeOH. An internal standard solution (50 μL of 1 μM cholic acid-d_5 solution) and 5% NH_4OH in cold acetonitrile (ACN) were added to the homogenate. The solution was then incubated for 1 hr at room temperature with gentle shaking. Fifty μL of serum was mixed with cold ACN and an internal standard solution. The sample solution was centrifuged at 13,000 rpm for 10 min at 4℃. The supernatant was collected and dried using a vacuum centrifuge. The dried matter was stored at –20℃ and reconstituted with 50% MeOH before LC-MS / MS analysis. Lipid levels of BAs were determined using an LC-MS / MS system. A reverse-phase column (Pursuit5 C18, 150 × 2.1 mm) was used with mobile phase A (7.5 mM ammonium acetate, pH 4 using 10 M acetic acid) and mobile phase B (5% CAN in MeOH). The LC was run at 200 μL/min and 24℃. Multiple reaction monitoring (MRM) was performed under negative ion mode, and the extracted ion chromatogram corresponding to the specific transition for each BA was used for quantification. The calibration range for each lipid was 0.1–10000 nM ($r^2 \geq 0.99$). Data analysis was performed using either Analyst 1.5.2.

Total bile acid analysis

According to the manufacturer's instruction, total BA was measured in serum and feces using the total BA assay kit (Crystal Chem). Fifty mg of the lyophilized feces was extracted in 4 mL of 75% (v/v) ethanol at 50℃ with gentle agitation for 2 hr. Fecal extracts after centrifugation were used to quantify the total BAs.

Bile salt hydrolase (BSH) activity assay

After feces were ground with PBS including 0.05% L-cystein hydrochloride (Sigma Aldrich) in a 100 μm strainer, 10 μL of the filtered solution was dropped onto DISK mounted on MRS agar containing 0.05% L-cystein hydrochloride, 0.5% taurodeoxycholic acid (Sigma-Aldrich), and 0.37 g/L CaCl (Sigma Aldrich). Plates were incubated under anaerobic conditions at 37℃ for 72 hours. The activity of BSH was analyzed by measuring the diameter of the precipitated colonies.

Statistical analysis

GraphPad Prism software (GraphPad) was used for statistical analyses. Significant differences between the two groups were analyzed with a two-tailed unpaired *t*-test. Multiple groups were analyzed by one- or two-way ANOVA followed by Bonferroni's post hoc test (*, $p < 0.05$; **, $p < 0.01$; ***, $p < 0.001$).

Results

HFD leads to pathological conditions in colon.

To address the impact of high fat on colon physiology, mice were fed a NCD, PD, or HFD for 2 months. The previous study has clarified that there are significant differences between a refined diet and a chow diet in terms of gut microbiota composition and host physiology [46]. PD and HFD commonly contain insoluble fiber (Figure 5A), which is generally not fermented by gut microbiota, and mice fed with insoluble fiber have significantly different microbial communities compared to those fed with soluble fiber [63]. Therefore, PD were adopted as control diet of HFD to exclude the effects of other dietary factors except fat. HFD contains 20% kcal carbohydrate, 60% kcal fat, and 20% kcal protein whereas PD contains 64% kcal carbohydrate, 16% kcal fat, and 20% kcal protein (Figure 5B). As reported, I observed higher body weight in mice fed HFD compared to those fed NCD or PD (Figure 5C). Unexpectedly, shorter colon lengths were found in mice fed the PD and HFD compared with mice fed the NCD (Figure 6A). I further addressed pathological changes of the colon by HFD feeding in a steady-state condition. Histopathology score of the colon was significantly higher in the HFD-fed mice than those in the PD- or NCD-fed mice (Figure 6B). In addition, shorter crypt lengths and reduced numbers of goblet cells were found in the HFD-fed mice (Figure 6C). Gut permeability measured by serum dextran levels was higher in the HFD-fed mice than in the PD- or NCD-fed mice (Figure 6D). Of note, significant alteration of colon pathology was also detected in the PD-fed mice compared with those in the NCD-fed mice (Figure 6). To confirm whether HFD accelerates tumorigenesis as reported previously [30, 47], I administered AOM and DSS to each diet-fed mice to induce inflammation-driven CRC (Figure 7A). Almost all HFD-fed mice died within a few days of treatment with AOM (10 mg/kg body weight), whereas all NCD-fed mice survived (Figure 7B). Additionally, PD-fed mice had a lower survival rate than NCD-fed mice (Figure7B). The surviving HFD-fed mice (n=2 / 10) possessed more polyps in the colon than mice fed the NCD or PD (Figure 7C). Similar to the steady-state, the colon length of mice fed the PD and HFD was shorter than that of mice fed the NCD (Figure 7C). Overall, I confirmed that the HFD induced pathological changes and promoted inflammation-induced tumorigenesis in the colon.

Feeding of the PD caused mild pathological changes in the colon; therefore, I adopted the PD as a control for the subsequent experiments.

A

Ingredient	Purified diet g/kg
Casein	200
L-Cystine	3
Corn Starch	397.49
Maltodextrin 10	132
Sucrose	100
Solka Floc (Insoluble fiber)	50
Soybean Oil	70
Lard	0
Mineral & Vitamin	47.5
t-Butylhydroquinone	0.01
Total	1000

Ingredient	High fat diet g/kg
Casein	200
L-Cystine	3
Corn Starch	0
Maltodextrin 10	125
Sucrose	72.8
Solka Floc (Insoluble fiber)	50
Soybean Oil	25
Lard	245
Mineral & Vitamin	53
Dye	0.05
Total	773.85

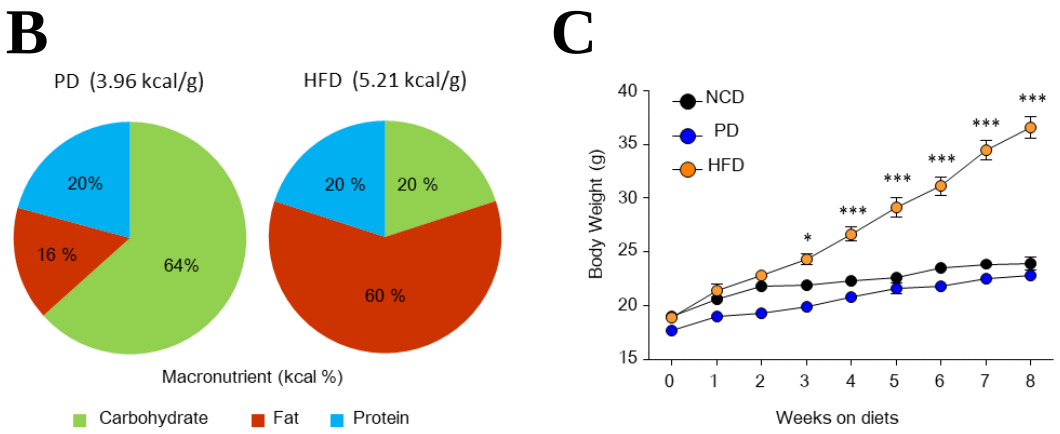

Figure 5. Dietary composition and alteration of body weight. (A) Composition of diet nutritional composition in purified diet (PD) and high-fat diet (HFD). (B) Macronutrient proportions in PD and HFD. (C) Changes of body weight for 2 months from mice PD- and HFD- mice. Data are presented as mean ± SD; comparisons were made by two-tailed *t*-test. **p* < 0.05, ****p* < 0.001. n = 5 mouse / group.

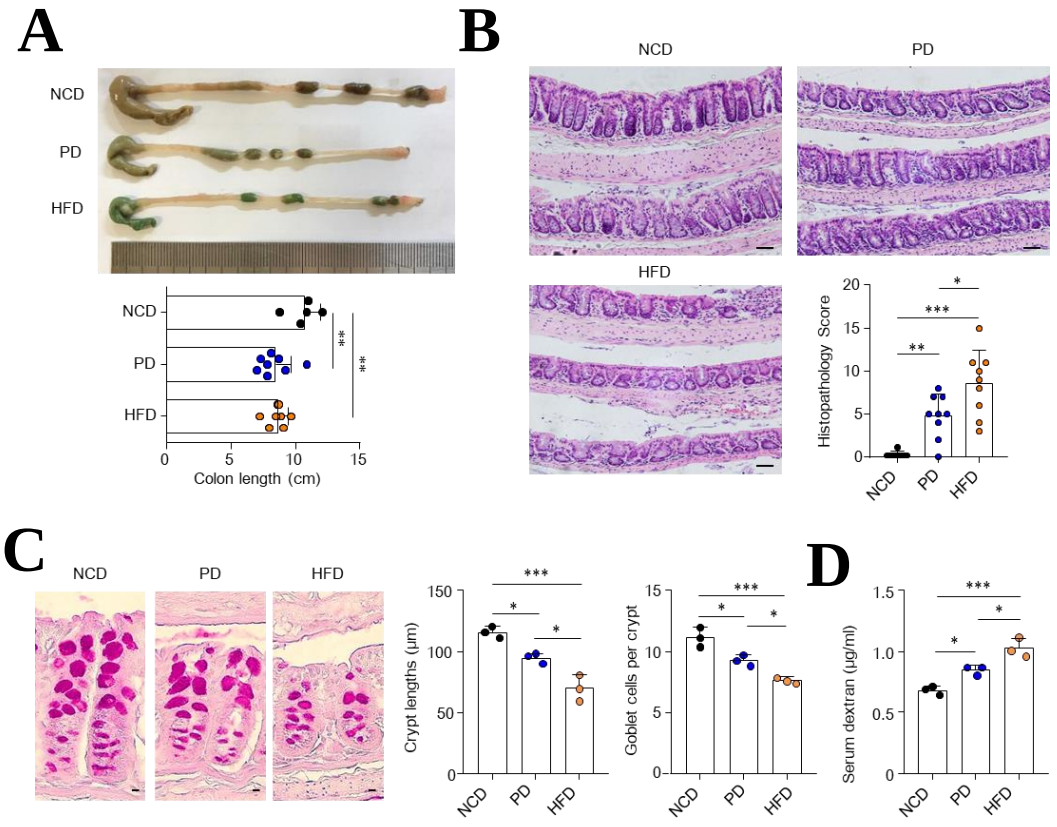

Figure 6. HFD resulted in pathological conditions in the colon. (A) Representative colon image and measurement of colon length from NCD-, PD-, and HFD-fed mice for 2 months. (B) Representative hematoxylin and eosin (H&E) staining image and histopathology score from colon tissues. Scale bar = 50 μm. (C) Representative periodic acid-Schiff (PAS) staining image, crypt lengths, and goblet cell number per crypt score from colon tissues. The crypt lengths and goblet cell number were measured at ≥ 35 crypts. Scale bar = 5 μm. (D) Measurement of FITC in serum after FITC-dextran administration to PD- and HFD-fed mice. Data are presented as mean ± SD; comparisons were made by two-tailed *t*-test. **p* < 0.05, ***p* < 0.01, ****p* < 0.001. Data were repeated two times in independent experiments.

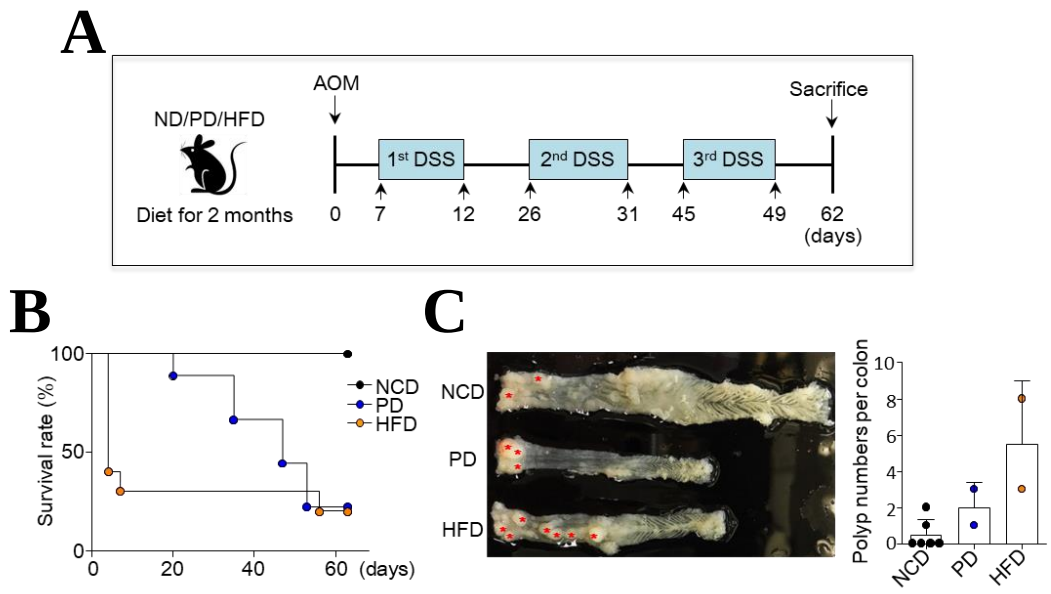

Figure 7. Increased incidence rate of colorectal cancer in HFD-fed mice. (A) Scheme of inflammation-induced colon tumorigenesis model made by AOM/DSS treatment after diet for 2 months. (B) Survival rate of PD- and HFD-fed mice after AOM/DSS treatment. (C) Representative image of colon and polyp numbers per colon. Red asterisks indicate polyps. Data information: Data are presented as mean ± SD; comparisons were made by two-tailed *t*-test. Data were repeated two times in independent experiments.

HFD amplifies CD44 expression and Wnt signaling in colonic crypts

Next, I investigated the effects of a HFD on colonic crypts regeneration by assessing the ability of isolated colonic crypts to form organoids in an ex vivo 3-D culture system. In line with previous results [30], mice fed a HFD produced significantly enhanced organoids in size and formation compared with those fed the PD (Figure 8A). In addition, Ki67-positive proliferating cells in the ISC and progenitor-dense crypt region of the colon increased significantly in HFD-fed mice compared with PD-fed mice (Figure 8B). Based on the activity of crypt regeneration, I examined the expression levels of ISC markers, leucine-rich-repeat-containing G-protein-coupled receptor 5 (Lgr5) and CD44, in the colonic crypt of PD- and HFD-fed mice. Although expression levels of *Lgr5* did not differ (Figure 9A), *CD44* expression was significantly higher in the colonic stem cell regions of HFD-fed mice than those in PD-fed mice (Figure 9B). Interestingly, previous studies have identified various isoforms of the CD44, which are formed by mRNA splicing and are known as CSC markers for CRC [64, 65]. I found that the numbers of CD44-positive cells and CD44 variant isoforms (CD44v) were augmented in the colonic crypts of the HFD-fed mice than in the PD-fed mice (Figure 9C and 9D). In addition, representative CSC markers (i.e., *CD24*, *CD166*, and *Ephb2*) increased significantly in the colonic crypts of HFD-fed mice compared to those in PD-fed mice (Figure 9E). However, mRNA expression associated with deep crypt secretory cell markers, EGF, and Notch signaling, which supports ISC maintenance, showed no difference or decreased (Figure 10). Among Wnt/β-catenin-related genes, *Cyclin D1*, *Axin2*, and *Apc* were significantly higher in HFD-fed mice than in PD-fed mice (Figure 11A). Hyper expression levels of *Axin2* in the colon of HFD-fed mice were confirmed with *in situ* hybridization (Figure 11B). I next assessed higher nuclear β-catenin accumulation in the colonic crypts of HFD-fed mice compared with those of PD-fed mice (Figure 11C). These results support the notion that a HFD increases stemness and expression of CSC markers through over-expression of Wnt/β-catenin signaling in the colonic crypt.

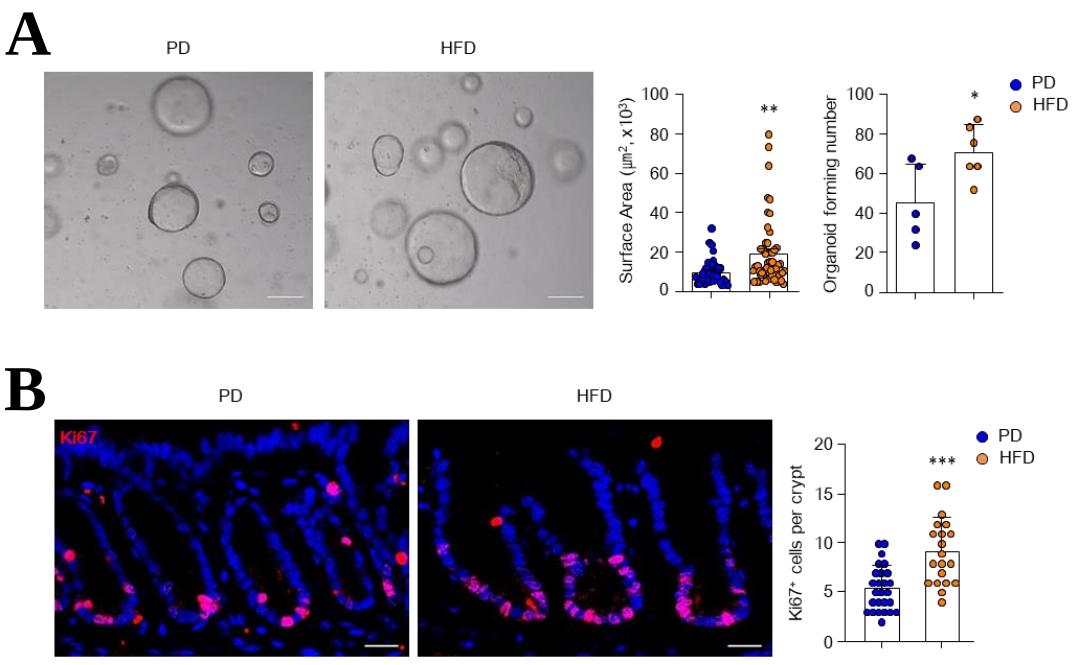

Figure 8. HFD stimulated proliferation of crypt cells. (A) Colon organoids were cultured from PD- and HFD-fed mice. Scale bar = 200 μm. Surface area and the forming number of organoids were measured. Surface area was measured at ≥ 70 organoids. (B) Immunofluorescence image of nuclei (blue) and Ki67 (red) in colon and quantification of Ki67 positive cells from the confocal image. Scale bar = 20 μm. Data are presented as mean ± SD; comparisons were made using the two-tailed *t*-test or two-way ANOVA multiple test. **p* < 0.05, ***p* < 0.01, ****p* < 0.001. Data were repeated twice in independent experiments.

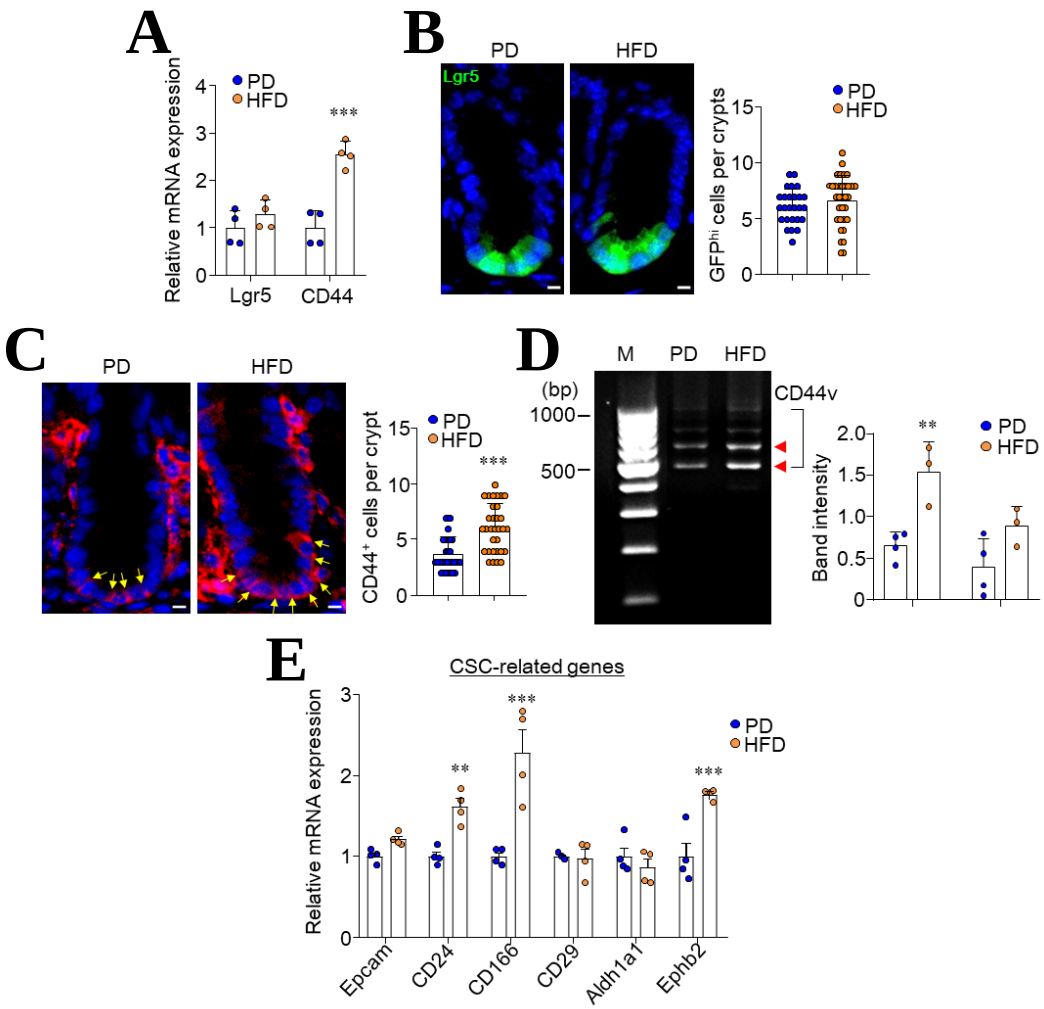
A
Relative mRNA expression
PD
HFD
***
Lgr5
CD44
B
PD
HFD
Lgr5
GFPhi cells per crypts
C
PD
HFD
CD44+ cells per crypt
D
M
PD
HFD
(bp)
1000
500
CD44v
Band intensity
**
E
CSC-related genes
Relative mRNA expression
Epcam
CD24
CD166
CD29
Aldh1a1
Ephb2

Figure 9. HFD induced abnormal stemness and CSC. (A) Relative mRNA expression levels of genes related to ISCs were measured by real-time PCR in the colonic crypts. (B) Immunofluorescence image of nuclei (blue) and Lgr5 (green) in the colon of PD- and HFD-fed *Lgr5-EGFP* mice and quantification of GFP^{high} cells in the crypts. Scale bar = 5 μm. (C) Immunofluorescence image of nuclei (blue) and CD44s-v (red) in the colon and quantification of CD44 positive cells per crypts from the confocal image. CD44 antibody recognizes an epitope on both CD44 standard forms (CD44s) and CD44 isoforms (CD44v). Yellow arrows indicate CD44 positive cells. Scale bar = 20 μm. (D) Real-time PCR analysis of total mRNA from colonic crypts of PD- and HFD-fed mice for primers targeted to exon 5 and 16 of the *CD44*. M = DNA size marker. (E) Relative mRNA expression levels of genes related to CSC markers were measured in the colonic crypts. Data are presented as mean ± SD; comparisons were made using the two-tailed *t*-test or two-way ANOVA multiple test. **p* < 0.05, ***p* < 0.01, ****p* < 0.001. Data were repeated twice in independent experiments.

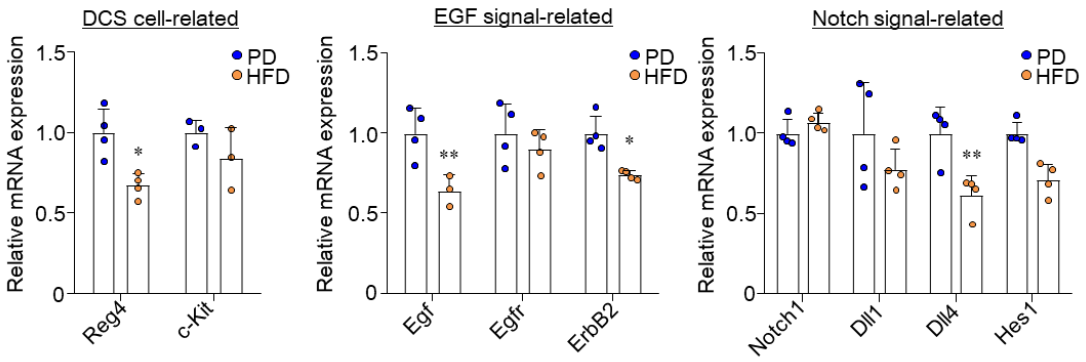

Figure 10. The expression level of various ISC niche signal–related genes. Relative mRNA expression levels of genes related to deep crypt secretory cells (DCS), EGF, and Notch signals were measured in the colonic crypts. Data are presented as mean ± SD; comparisons were made using the two-tailed *t*-test or two-way ANOVA multiple test. **p* < 0.05, ***p* < 0.01. Data were repeated twice in independent experiments.

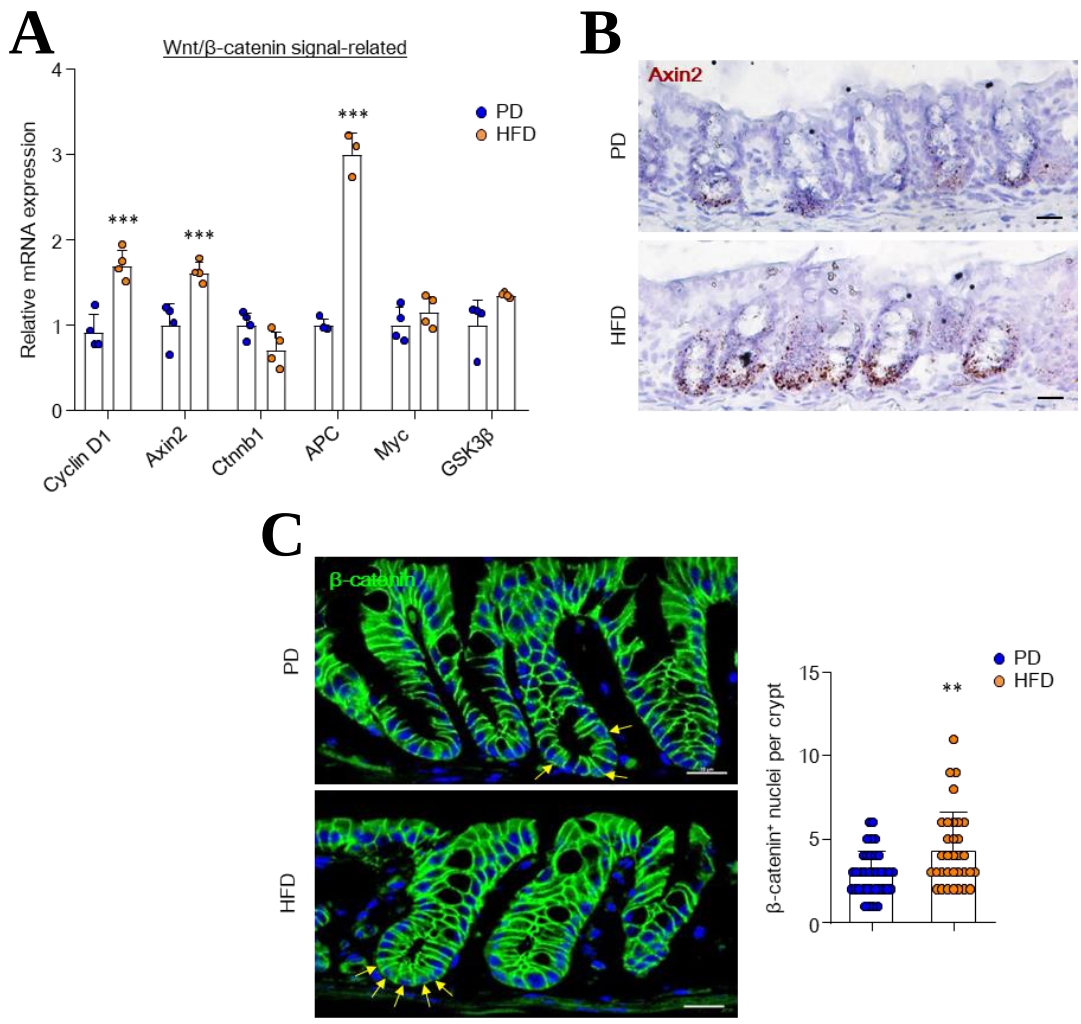

Figure 11. HFD amplified Wnt/β-catenin signaling in colonic crypts. (A) Relative mRNA expression levels of genes related to Wnt signaling pathways were measured by real-time PCR in the colonic crypts. (B) Representative images show *Axin2* in situ hybridization in the colon. Scale bar = 20 μm. (C) Immunofluorescence image of nuclei (blue) and β-catenin (green) in colon and quantification of nuclear β-catenin localization from the confocal image. Yellow arrows indicate nuclear translocation of β-catenin. Scale bar = 20 μm. Data are presented as mean ± SD; comparisons were made using the two-tailed *t*-test or two-way ANOVA multiple test. $^{**}p < 0.01$, $^{***}p < 0.001$. Data were repeated twice in independent experiments.

HFD stimulates Wnt2b production and cancer-associated properties in colonic MSCs

I hypothesized that colonic MSCs could potentially activate Wnt/β-catenin signaling under conditions of a HFD. Higher expression of *Wnt2b* was determined in the subepithelium and submucosa of the colon, where MSCs are usually localized, from mice fed with a HFD than from mice eating a PD (Figure 12A). On the other hand, there was a slight increase in *Wnt5a* in the colon subepithelium of mice fed a HFD, but not other Wnt family members (i.e., *Wnt2*, *Wnt3*, *Wnt4*, *Wnt6*, *Wnt9b*) (data not shown). *Wnt2b* expression was primarily observed in the presence of ISC and progenitor cells in the crypt bottom; therefore, Wnt2b rather than Wnt5a may play an essential role in the maintenance and development of colonic stem cells. Recent studies have suggested that $gp38^{+}CD90^{+}$ MSCs produce Wnt2b, a critical growth factor for ISC maintenance [66]. Therefore, I assessed the Wnt2b expression levels in colonic $CD90^{+}$ MSCs. Of interest, Wnt2b production was significantly higher in colonic MSCs isolated from mice fed a HFD than PD-fed mice (Figure 12B). FACS and IHC analysis revealed higher numbers of $gp38^{+}CD90^{+}$ MSCs in the subepithelial region of mice fed a HFD than a PD (Figure 13A and 13B). To further investigate the alteration of colonic MSCs by HFD, I performed RNA-sequencing experiments. Among the 290 genes that differ significantly between the two groups, 226 were upregulated in colonic MSCs from HFD-fed mice compared with PD-fed mice (Figure 14A). Notably, predominant levels of *CXCR4* and *IL1RL1* expression, which are known to activate MSCs to CAFs [67, 68], were identified in colonic MSCs by HFD feeding. KEGG pathway analysis of HFD-derived MSCs showed an upregulation of the PI3K-Akt signaling pathway, focal adhesion molecules, ECM-receptor interaction, cell adhesion molecules, and the calcium signaling pathway (Figure 14B). In gene set enrichment analysis (GSEA), I found increased expression of *Sox2* in colonic MSCs from HFD-fed mice (Figure 14C), which reportedly promotes tumorigenesis [69]. I then measured the oxygen consumption rate (OCR; an indicator of oxidative phosphorylation) and extracellular acidification rate (ECAR; an indicator of glycolysis) to fully assess the effects of a HFD on the energy metabolism of colonic MSCs. Although there was no significant difference in OCR level (data not shown), ECAR level after treatment with glucose was enhanced in HFD-derived MSCs compared with PD-derived MSCs (Figure 15).

In addition, as parameters of glycolysis stress, glycolysis, glycolytic capacity, and non-glycolytic acidification increased in colonic MSCs after HFD feeding (Figure 15). Considering these results, I concluded that HFD stimulates colonic MSC expansion, Wnt2b production, and cancer-associated properties.

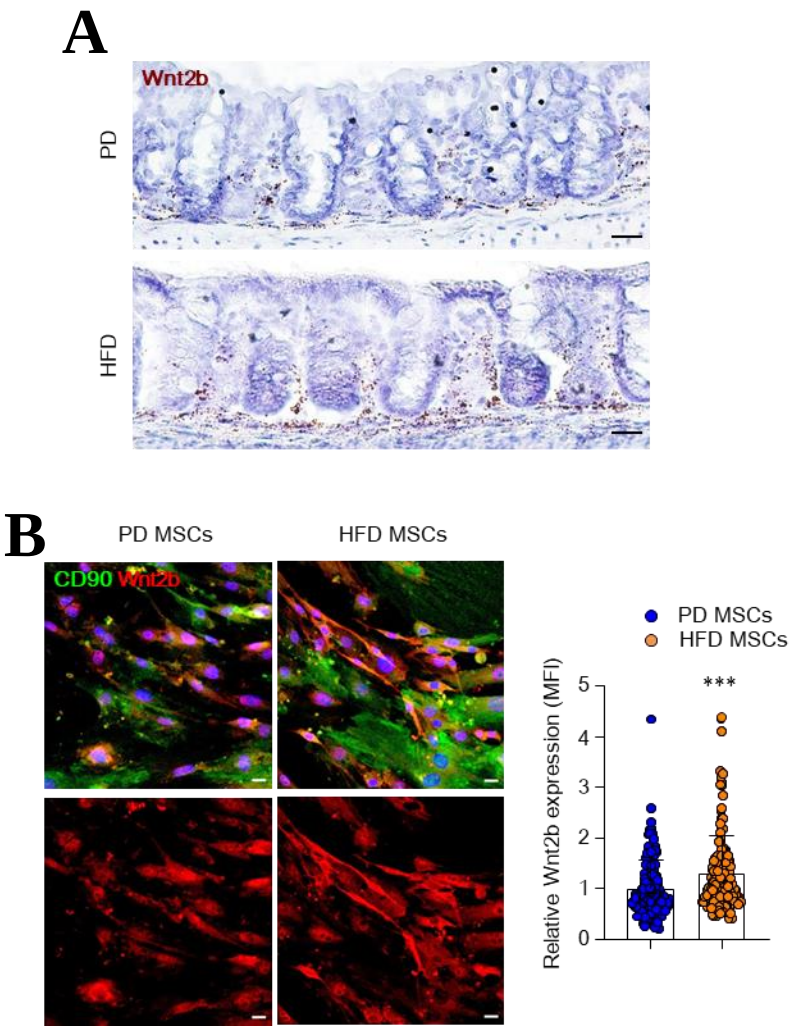

Figure 12. HFD promoted the Wnt2b production in colonic MSCs. (A) Representative images show *Wnt2b* in situ hybridization in the colon of mice fed PD or HFD. Scale bar = 20 μm. (B) Immunofluorescence image of nuclei (blue), CD90 (green), and Wnt2b (red) in MSCs and quantification of Wnt2b expression was measured through relative Wnt2b mean fluorescence intensity (MFI). Scale bar = 20 μm. ***$p < 0.001$. Data were repeated twice in independent experiments.

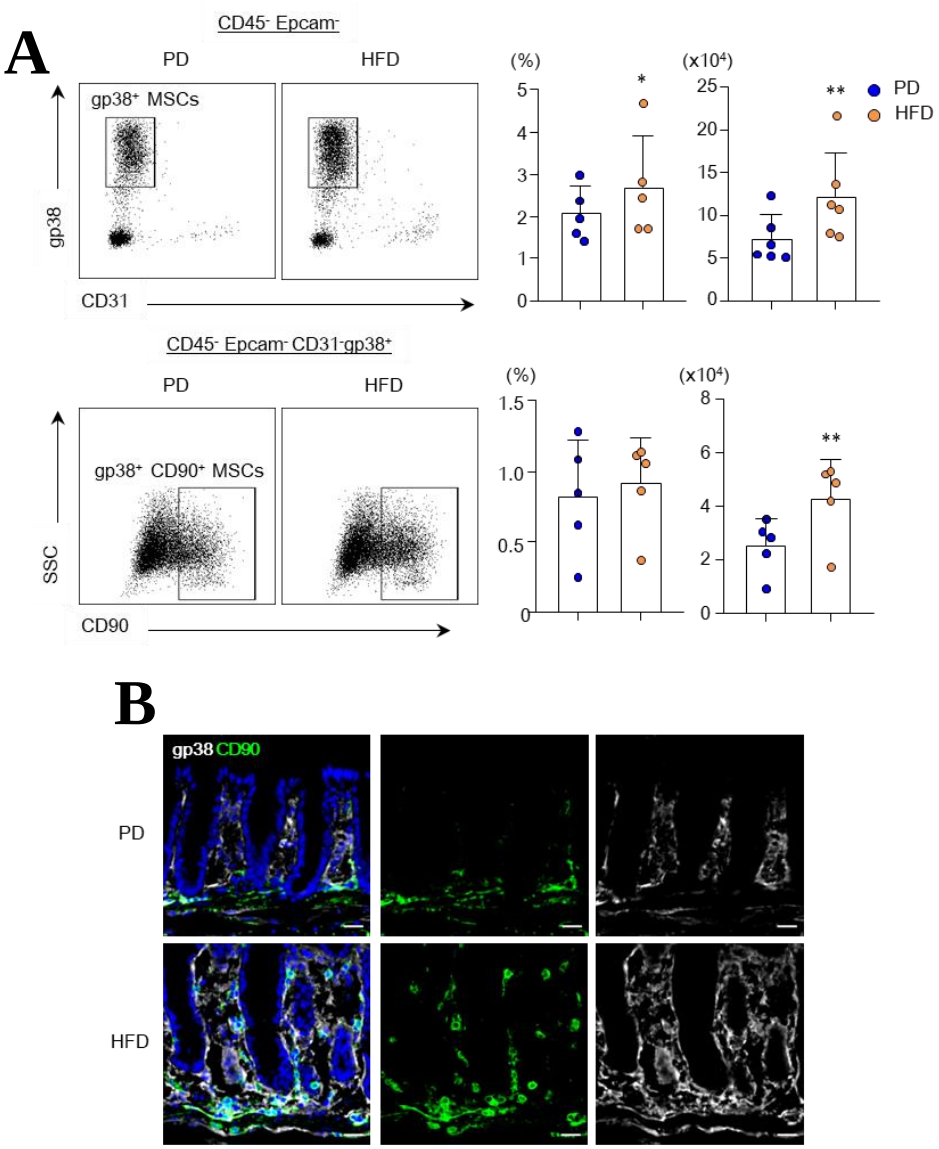

Figure 13. The expansion of sub-epithelial MSCs in colon of HFD-fed mice. (A) Representative FACS plots, percentages, and absolute numbers of gp38^{+} MSCs and gp38^{+} CD90^{+} MSCs in total recovery cells. (B) Immunofluorescence image of nuclei (blue), CD90 (green), and gp38 (white) in the colon of mice fed a PD or HFD. Scale bar = 20 μm. Data are presented as mean ± SD; comparisons were made with the two-tailed *t*-test. **p* < 0.05, ***p* < 0.01. Data were repeated twice in independent experiments.

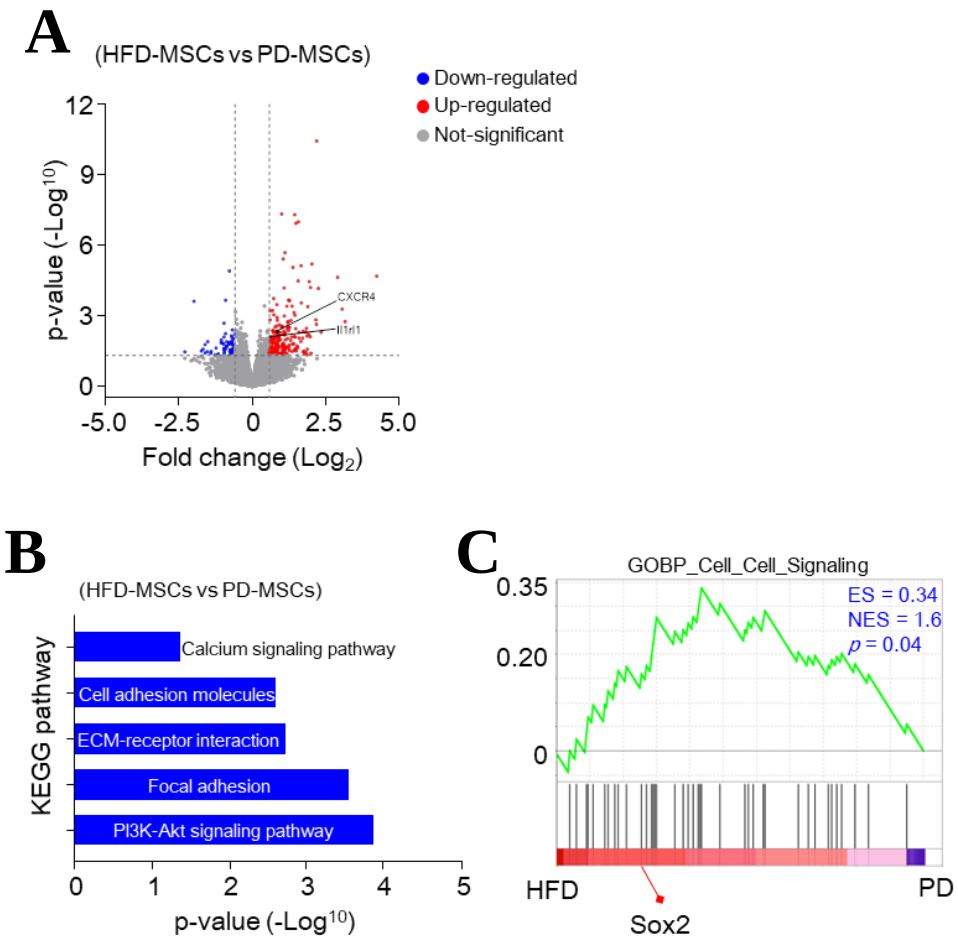

Figure 14. HFD-derived colonic MSCs have the CAF-like properties. RNA-seq analysis of colonic MSCs from PD- and HFD-fed mice (n=3/group). (A) Volcano plots of all genes based on their log2 fold-change and p-values. Differentially expressed genes (fold-change ≥ |1.5|; $p < 0.05$) were sorted. (B) KEGG pathway analysis through gProfiler (fold-change ≥ 1.5; $p < 0.05$). (C) Gene set enrichment analysis (GSEA) in colonic MSCs (fold-change ≥ 1.5). Enrichment score (ES), normalized enrichment score (NES), and p-values are stated in the panel, and representative genes are indicated under the panel. Data are presented as mean ± SD; comparisons were made with the two-tailed *t*-test.

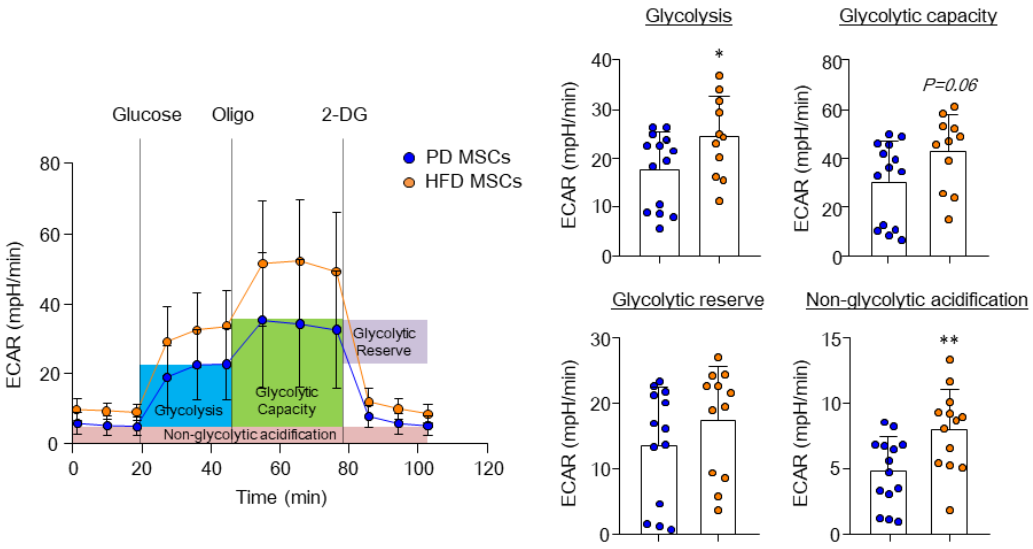

Figure 15. HFD enhanced glycolytic activity in colonic MSCs. The extracellular acidification rate (ECAR) of colonic MSCs was measured in response to injection of glucose, oligomycin (Oligo), and 2-deoxy-glucose (2-DG) under basal conditions. Parameters of glycolysis stress were measured from the ECAR of colonic MSCs. Data are presented as mean ± SD; comparisons were made with the two-tailed *t*-test. **P* < 0.05, ***P* < 0.01. Data were repeated twice in independent experiments.

HFD-derived MSCs induces CSCs characteristics in colon organoids

I next investigated whether HFD-derived MSCs promote colon organoid growth and formation. In the presence of ENR medium, HFD-derived MSCs increased both size and formation of organoids compared with PD-derived MSCs (Figure 16A). I next investigated whether colonic MSCs from HFD-fed mice directly stimulated Wnt/β-catenin signaling and CSC markers expression. The Wnt signal target genes were analyzed from colon organoids co-cultured with MSCs obtained from each group of mice. *Axin2*, *Ctnnb1*, and *Apc* expression had increased significantly in organoids co-cultured with MSCs from HFD-fed mice compared with those from PD-fed mice (Figure 16B). Of note, higher mRNA levels of *CD44* and *Ephb2* were observed in organoids co-cultured with HFD-derived MSCs than in PD-derived organoids (Figure 16C). To examine whether HFD-derived colonic MSCs promote tumorigenesis, I co-cultured the colon organoids derived from $Apc^{Min/+}$ mice with colonic MSCs from each group of mice. Co-culture with HFD-derived MSCs promoted the size and formation of colon organoids derived from $Apc^{Min/+}$ mice in the presence of EN medium (Figure 16D). To clarify the effect of Wnt proteins secreted by MSCs on tumorigenic organogenesis, Wnt secretion inhibitors (i.e., C59) were added to the ENR medium. As anticipated, the growth of organoids co-cultured with MSCs of HFD-fed mice decreased significantly similar to as much as organoids co-cultured with MSCs of PD-fed mice (Figure 17). These results indicate that HFD promotes proliferation of ISCs and CSCs through stimulation of Wnt2b secretion by colonic MSCs.

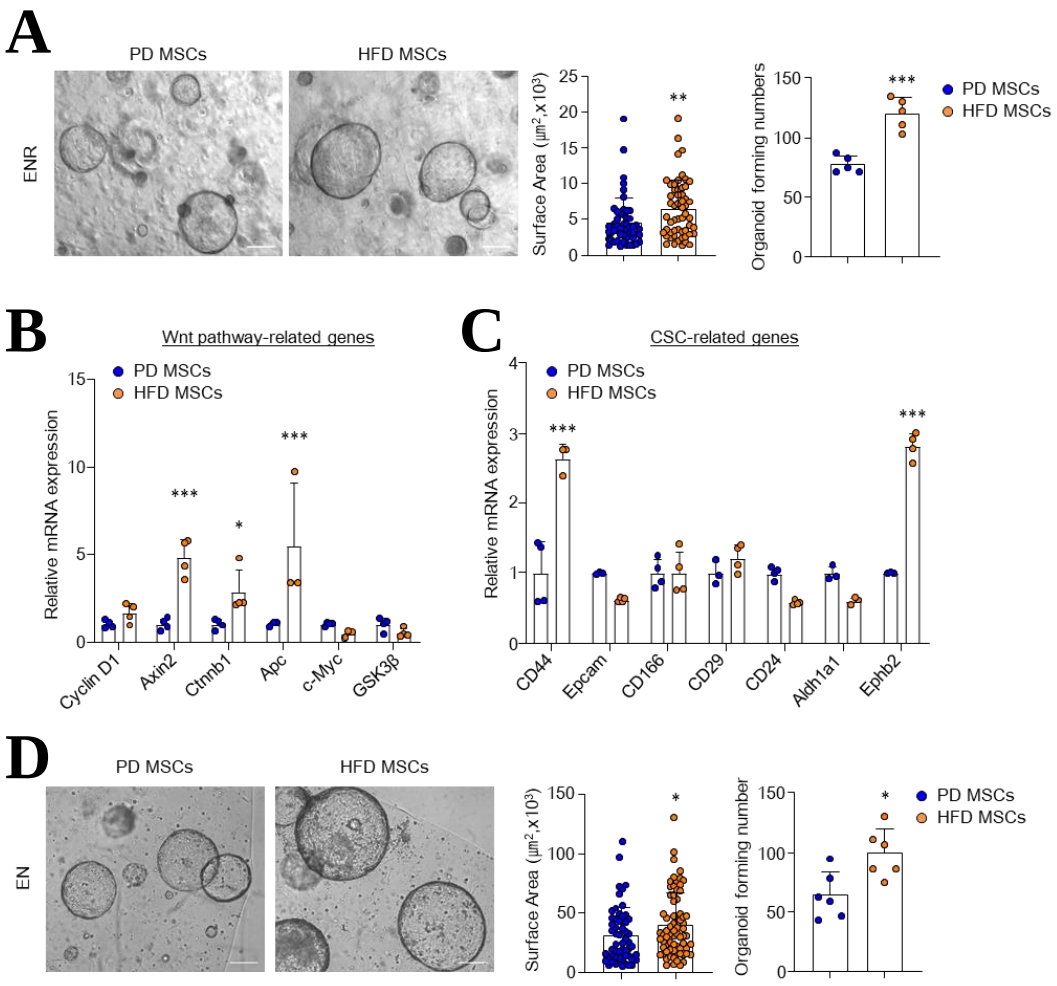
A
PD MSCs
HFD MSCs
ENR
Surface Area (μm² x 10³)
Organoid forming numbers
PD MSCs
HFD MSCs
B
Wnt pathway-related genes
Relative mRNA expression
Cyclin D1
Axin2
Ctnnb1
Apc
c-Myc
GSK3β
C
CSC-related genes
CD44
Epcam
CD166
CD29
CD24
Aldh1a1
Ephb2
D
EN
Organoid forming number

Figure 16. HFD-derived colonic MSCs stimulate proliferation and CSCs-related gene expression in colon organoids. (A) Colon organoids from naïve C57BL/6N mice were co-cultured with MSCs from PD- and HFD-fed mice in ENR medium. Scale bar = 200 μm. The surface area and forming number of organoids were measured. Surface area was measured at ≥ 50 organoids. (B) Relative mRNA expression levels of genes related to Wnt signal pathways were measured in the naïve colon organoids co-cultured with colonic MSCs. (C) Relative mRNA expression levels of CSC markers were measured in the naïve colon organoids co-cultured with colonic MSCs. (D) Colon organoids from $Apc^{Min/+}$ mice were co-cultured with MSCs in EN medium. Scale bar = 200 μm. The surface area and forming number of organoids were measured. Surface area was measured at ≥ 50 organoids. Data are presented as mean ± SD; comparisons were made by two-tailed *t*-test or two-way ANOVA multiple test. $*p < 0.05$, $**p < 0.01$, $***p < 0.001$. Data were repeated twice in independent experiments.

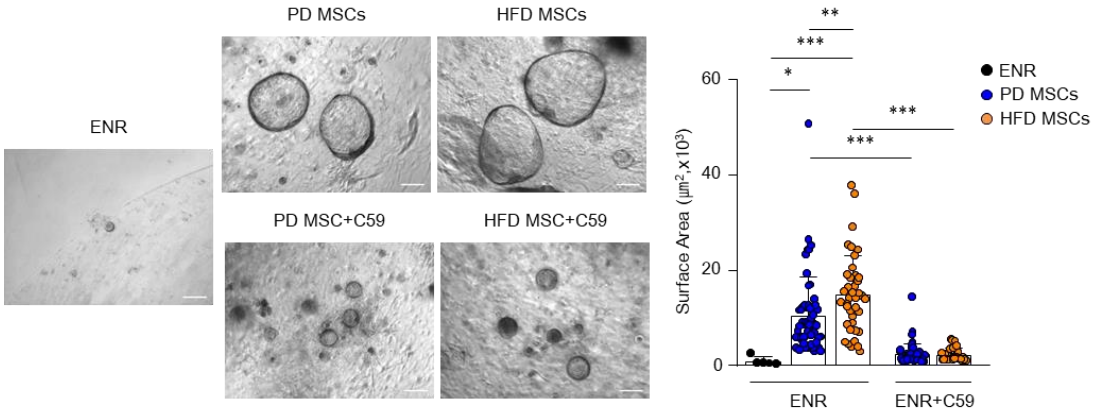

Figure 17. Effects of Wnt antagonists in the organogenesis by MSCs. Colon organoids from naïve C57BL/6N mice were co-cultured with MSCs in ENR medium or ENR containing C59 for 9 days. C59 was treated only for the final 2 days. Scale bar = 200 μm. The surface area of organoids was measured. Surface area was measured at ≥ 25 organoids. Data are presented as mean ± SD; comparisons were made by two-tailed *t*-test or two-way ANOVA multiple test. **p* < 0.05, ***p* < 0.01, ****p* < 0.001. Data were repeated twice in independent experiments.

Metabolites from altered gut microbiota by HFD caused hyper Wnt2b secretion from MSCs

Alteration of microbial metabolites by HFD feeding is associated with intestinal tumorigenesis [47]. Therefore, I next determined the regulation of gut microbial metabolites on MSC dysfunction in HFD-fed mice. Colonic MSCs were obtained from naïve C57BL/6N mice and treated with cecal microbial products (CMP) from PD- and HFD-fed mice. Interestingly, CMP from HFD-fed mice stimulated more Wnt2b expression by colonic MSCs than that from PD-fed mice (Figure 18A and 18B). I next analyzed the profiles of gut microbiota in the feces of PD- and HFD-fed mice. The results of the Shannon index, Chao1, and operational taxonomic units indicated that the diversity of resident gut microbiota decreased in the feces of HFD-fed mice compared with those of PD-fed mice (Figure 19A). Principal component analysis of unweighted and weighted UniFrac revealed clear separation of gut microbiota composition between PD- and HFD-fed mice (Figure 19B). In LEFSe taxonomic cladogram, the gut microbiota of HFD-fed mice was dominated by the *Firmicutes* and *Deferribacteres* phyla, with lower proportions of *Proteobacteria* and *Verrucomicrobia* phyla (Figure 19C). Interestingly, *Bacteroides vulgatus* increased significantly in HFD-fed mice compared with PD-fed mice at the species level (Figure 19D). Overall, these results imply that alteration of microbial metabolites by HFD feeding may drive the activation of colonic MSCs.

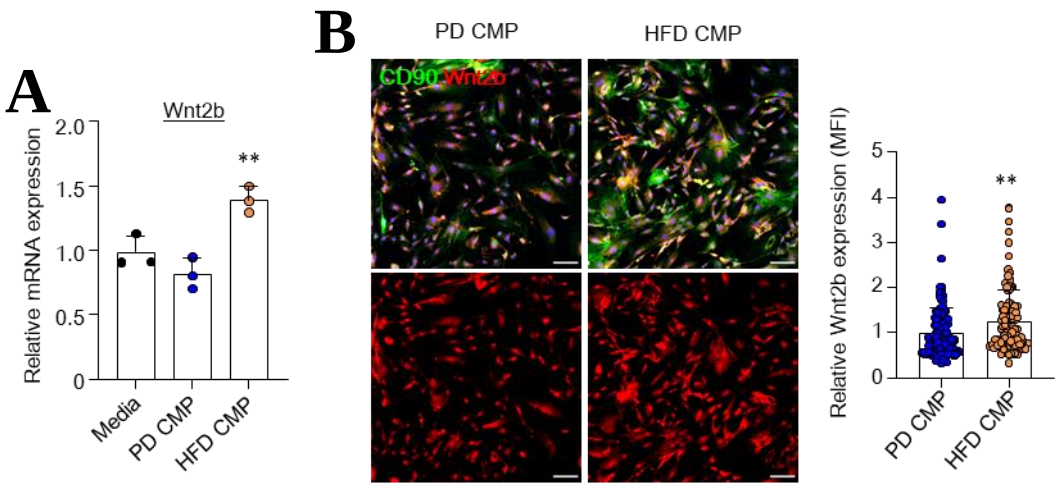

Figure 18. Regulation of Wnt2b by cecal microbial products. (A) Relative mRNA expression levels of *Wn2b* were measured in the naïve in vitro colonic MSCs treated with cecal microbial products (CMP) from PD- and HFD-fed mice. (B) Immunofluorescence image of nuclei (blue), CD90 (green), and Wnt2b (red) in the in vitro colonic MSCs treated with CMP and relative Wnt2b MFI was calculated based on the control group. Scale bar = 100 μm. Data are presented as mean ± SD; comparisons were made by two-tailed *t*-test or two-way ANOVA multiple test. $^{**}p < 0.01$. Data were repeated twice in independent experiments.

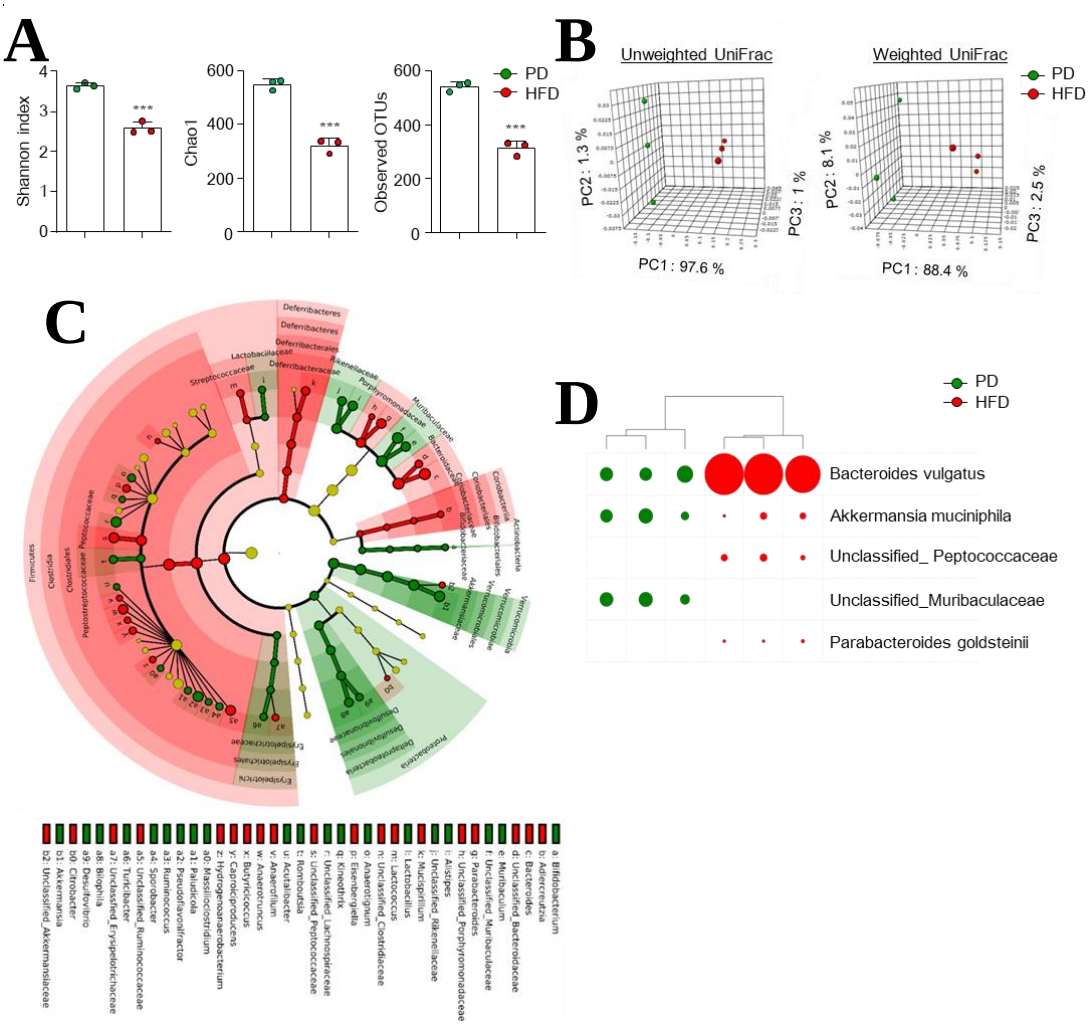
A
Shannon index
Chao1
Observed OTUs
PD
HFD
***
B
Unweighted UniFrac
Weighted UniFrac
PC1 : 97.6 %
PC2 : 1.3 %
PC3 : 1 %
PC1 : 88.4 %
PC2 : 8.1 %
PC3 : 2.5 %
C
D
Bacteroides vulgatus
Akkermansia muciniphila
Unclassified_ Peptococcaceae
Unclassified_Muribaculaceae
Parabacteroides goldsteinii

Figure 19. HFD led to a change in gut microbiota composition and community. Pyrosequencing analysis for gut microbiota following a HFD was determined from feces of PD- and HFD-fed mice. (A) Shannon index, Chao1, and Operational taxonomic units (OTUs) of fecal microbiota were determined. (B) Principal component analysis (PCA) of unweighted UniFrac and weighted UniFrac distances was analyzed for clustering fecal microbial communities. (C) Taxonomic cladogram from LEfSe and dot size means proportional to taxon abundance. (D) Comparison of bacterial ratio at the species level. Size of circle equates proportion in entire. Full size of circle = 45.41 %. Bacteria with a minimum ratio > 2 % only were compared. Data are presented as mean ± SD; comparisons were made by two-tailed *t*-test or two-way ANOVA multiple test. ***$p < 0.01$. Data were repeated twice in independent experiments.

Increased FFA by HFD does not affect the secretion of Wnt2b from MSCs

To identify the gut microbiota-derived metabolites that play a critical role, I analyzed short chain fatty acid (SCFA) in CMP of mice fed PD or HFD. There was no difference when SCFA level was compared in CMP of mice fed PD or HFD (Figure 20). I thus investigated whether FFA by HFD induces dysfunction in MSCs. I first analyzed free fatty acids (FFAs) in the CMP. As expected, overall the proportion of FFAs was significantly higher in the CMP of HFD-fed mice compared with those from PD-fed mice (Figure 21). As reported previously [30], each FFA, (i.e., palmitic acid, oleic acid, stearic acid, and the mixture combination) enhanced colon stemness (Figure 22A). However, each FFA could not stimulate *Wnt2b* expression from MSCs (Figure 22B).

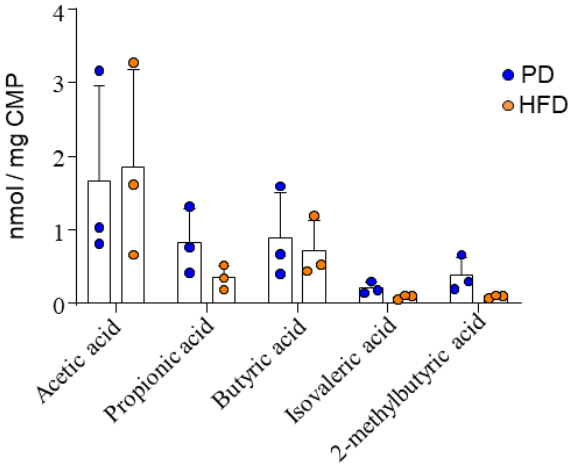

Figure 20. The analysis of short-chain fatty acid. The level of short chain fatty acid (SCFA) in CMP of mice fed PD or HFD.

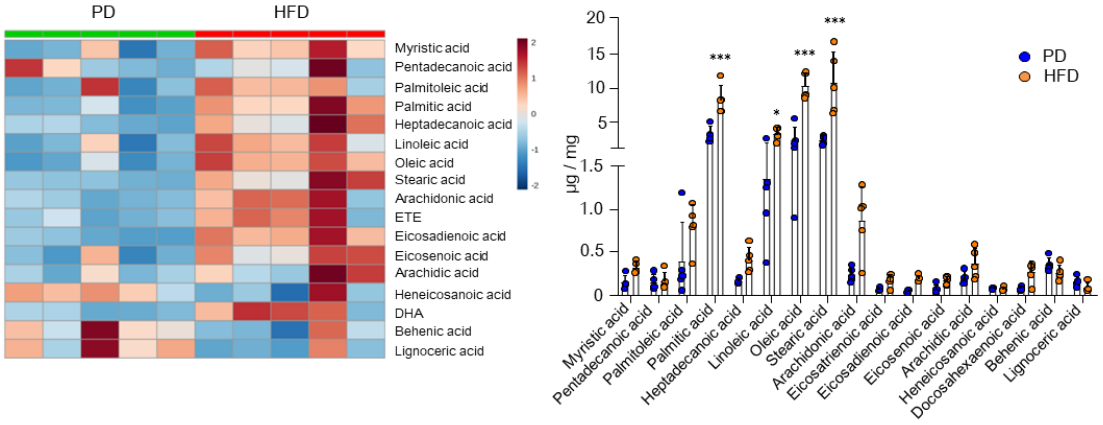

Figure 21. The increased FFA level in CMP of mice fed HFD. Heat map (left) and quantification (right) of FFA levels were analyzed in the CMP of PD- and HFD-fed C57BL/6N mice for 5 months. Data are presented as mean ± SD; comparisons were made with the two-tailed t-test or two-way ANOVA Bonferroni's multiple test. *$p < 0.05$, ***$p < 0.001$. Data were repeated twice in independent experiments.

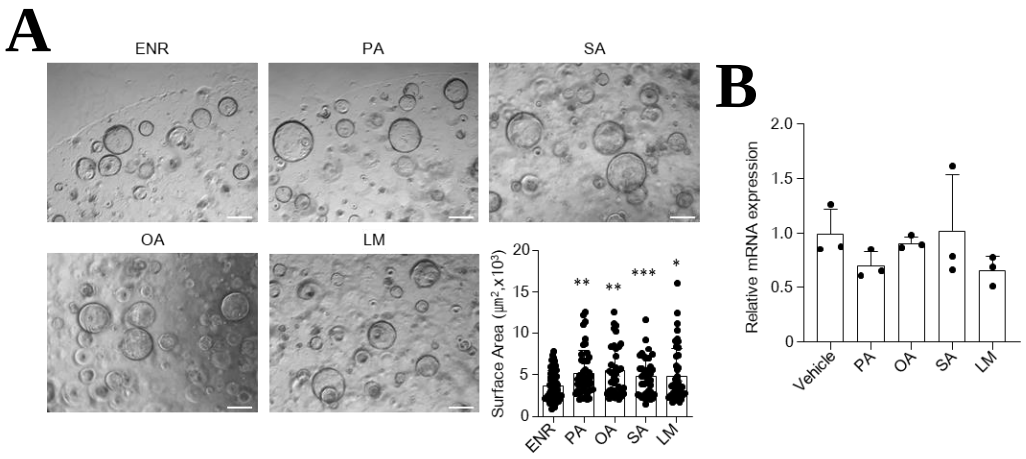

Figure 22. FFA did not promote Wnt2b production from colonic MSCs. (A) Colon organoids of naïve C57BL/6N mice were cultured with palmitic acid (PA; 30 μM), stearic acid (SA; 30 μM), oleic acid (OA; 30 μM), or lipid mixture (LM; 1%). Scale bar = 200 μm. The surface area was measured at ≥ 40 organoids. (B) Relative mRNA expression levels of *Wnt2b* were measured in the colonic MSCs treated with FFAs (30 μM PA, 30 μM OA, 30 μM SA, 1% LM). Data are presented as mean ± SD; comparisons were made with the two-tailed t-test or two-way ANOVA Bonferroni's multiple test. *$p < 0.05$, **$p < 0.01$, ***$p < 0.001$. Data were repeated twice in independent experiments.

HFD-derived gut microbiota increased the BA metabolites

I next considered bile acids (BAs) as another candidate of gut microbiota-derived metabolites because HFD-induced BA dysmetabolism was associated with tumorigenesis in intestine and liver [56, 70]. I observed no difference in gallbladder weight between the PD- and HFD-fed mice (Figure 23A). Thus, I investigated potential differences in the amounts of BAs excreted from the gall bladder. Although there was no difference in serum BA levels, fecal BA excretion was significantly higher in HFD-fed mice than PD-fed mice (Figure 23B and 23C). I next cultured feces in MRS agar containing tauro-DCA to assess the activity of the bile salt hydrolase (BSH) responsible for BA deconjugation. As shown in Figure 23*D*, the tauro-precipitated colony was significantly larger in HFD-fed mice than in PD-fed mice. Therefore, I analyzed BA composition in serum and feces to determine whether a HFD affects BA metabolism by altering the gut microbiota. The proportion of secondary BAs (i.e., DCA and HDCA) in the serum was higher in HFD-fed mice than in PD-fed mice (Figure 24A). However, the proportion of deconjugated BAs (i.e., CA and CDCA) and secondary BAs (i.e., HDCA) in the feces was greater in the HFD-fed mice compared with the PD-fed mice (Figure 24B). These results demonstrated that a HFD expanded BSH-producing bacteria and subsequently increased the production of de-conjugated and secondary BAs.

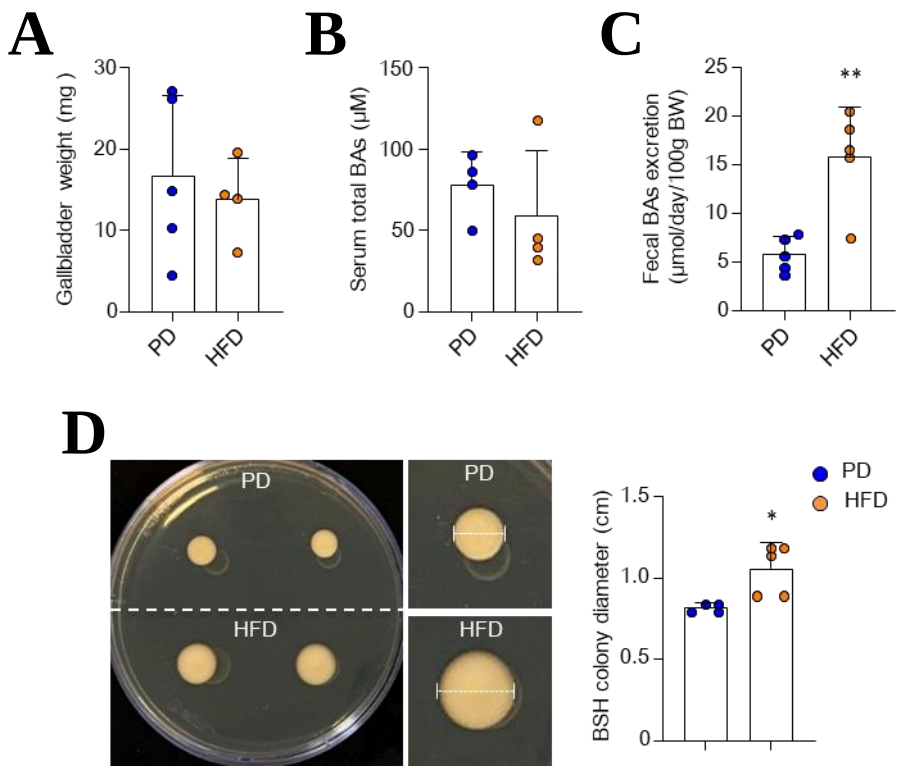

Figure 23. Expansion of bacteria with BSH activity induced by HFD. (A) Weights of gallbladders in mice fed a PD or HFD for 2 months. (B) Total BA levels were measured in the portal vein serum. (C) Total BA levels were measured in feces. Fecal BA excretion was calculated from fecal total BA levels. (D) Bile salt hydrolase (BSH) activity assay in feces. Data are presented as mean ± SD; comparisons were made with the two-tailed *t*-test or two-way ANOVA multiple test. **p* < 0.05, ***p* < 0.01. Data were repeated twice in independent experiments.

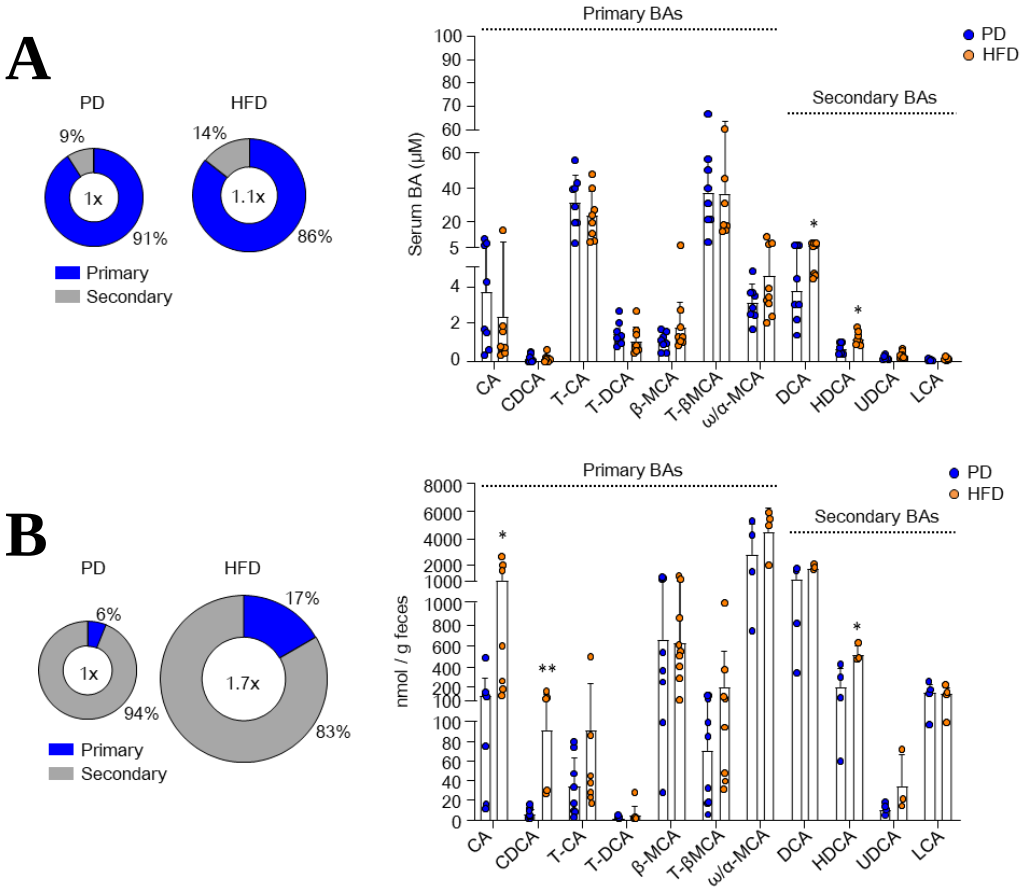

Figure 24. HFD alters the composition of BAs through gut microbiota. (A) Serum BA composition and individual BA levels were measured. (B) Fecal BA composition and individual BA levels were measured. Data are presented as mean ± SD; comparisons were made with the two-tailed *t*-test or two-way ANOVA multiple test. **p* < 0.05, ***p* < 0.01. Data were repeated twice in independent experiments.

BAs-FXR axis stimulates Wnt2b production in colonic MSCs

Based on the increased levels of BAs in HFD-fed mice, I investigated the expression levels of BA receptors in colonic MSCs. The proportion of all types of BA receptors (i.e., *VDR*, *TGR5*, and *FXR*) was significantly higher in colonic MSCs obtained from HFD-fed mice than those obtained from PD-fed mice (Figure 25A). Additionally, expression of FXR-target genes (i.e., *Ostα*, *Ostβ*, *Shp*, and *Ibabp*) increased significantly by HFD feeding (Figure 25B). I then co-cultured colonic MSCs with CDCA or DCA, natural ligands with a high affinity for BA receptors, and analyzed the expression of Wnt2b to determine the effects of BAs on Wnt2b secretion from colonic MSCs. CDCA treatment greatly increased the expression of *Wnt2b* from colonic MSCs isolated from naïve mice in a dose-dependent manner (Figure 26A). I also found similar effects of DCA, another natural ligand for the BA receptor (Figure 26B). In addition, increased protein levels of Wnt2b expression by CDCA were also observed (Figure 26C). As CDCA and DCA are known to have an affinity for both FXR and TGR5 [71], I adopted specific agonists for FXR (i.e., GW4064) or TGR5 (i.e., INT-777) to identify the receptor signaling that primarily mediates increased Wnt2b expression *in vitro*. GW4064 significantly increased *Wnt2b* mRNA expression while INT-777 did not affect *Wnt2b*, indicating FXR rather than TGR5 plays a critical role in the Wnt2b production by HFD feeding (Figure 26D and 26E). Interestingly, HFD-derived MSCs promoted Wnt2b production to a greater extent than PD-derived MSCs in the presence of CDCA (Figure 26F and 26G). Overall, activation of BAs-FXR signaling stimulated Wnt2b production in colonic MSCs.

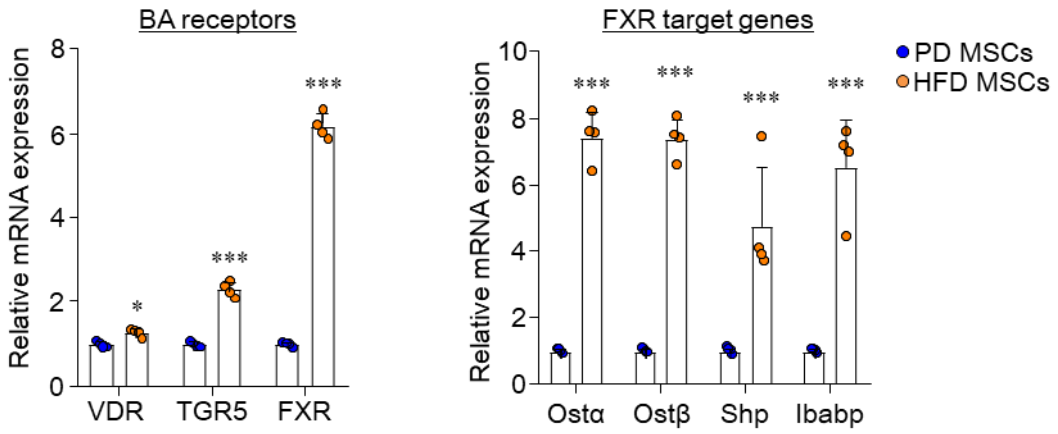

Figure 25. Activated FXR signal pathway in HFD-fed mice. Relative mRNA expression levels of genes related to BA receptors and FXR signaling target genes were measured in the colonic MSCs obtained from PD- and HFD-fed mice. Data are presented as mean ± SD; comparisons were made using the two-tailed *t*-test, one-way ANOVA, or two-way ANOVA multiple test. *$p < 0.05$, ***$p < 0.001$. Data were repeated twice in independent experiments.

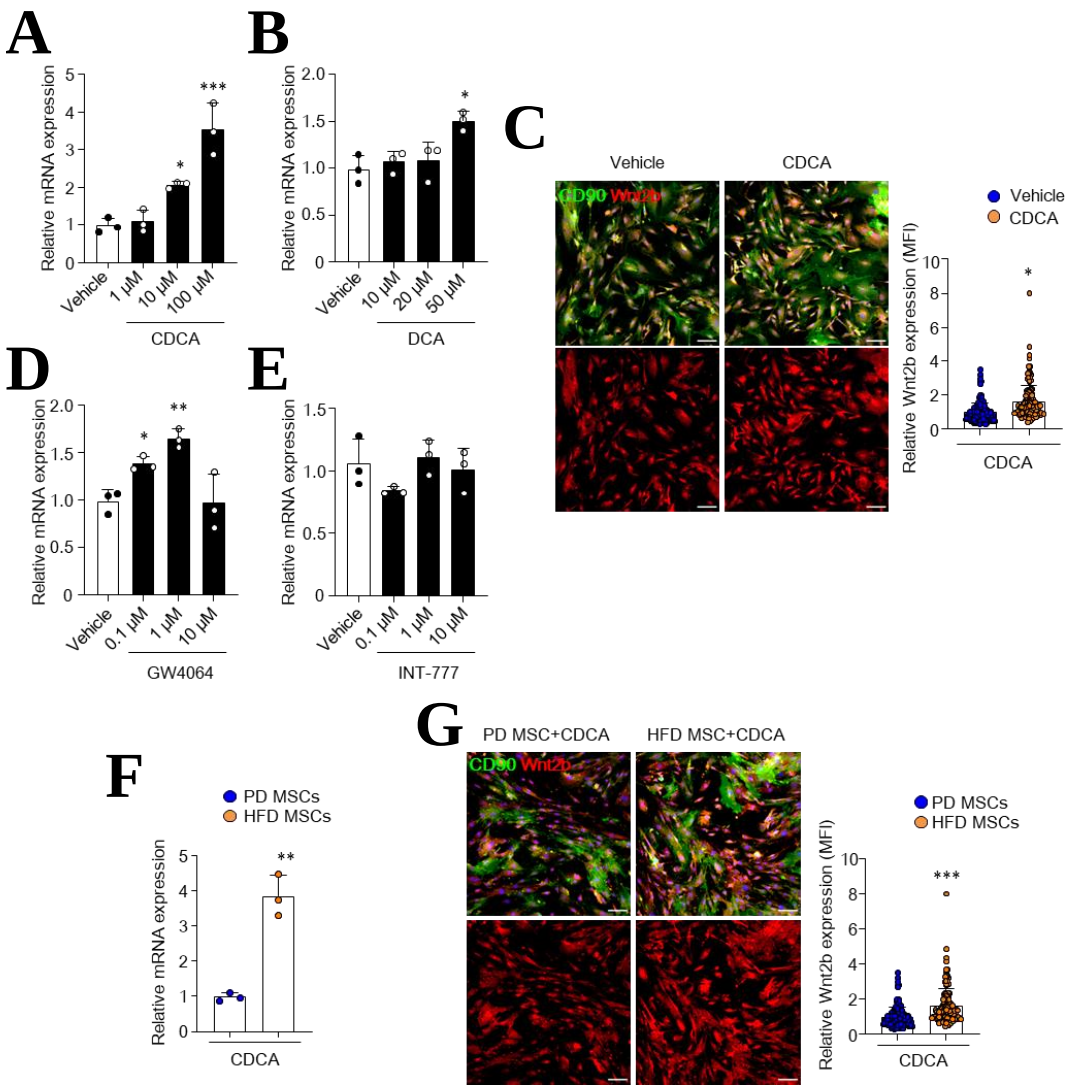
A
Relative mRNA expression
Vehicle
1 μM
10 μM
100 μM
CDCA
B
Relative mRNA expression
Vehicle
10 μM
20 μM
50 μM
DCA
C
Vehicle
CDCA
CD90 Wnt2b
Vehicle
CDCA
Relative Wnt2b expression (MFI)
CDCA
D
Relative mRNA expression
Vehicle
0.1 μM
1 μM
10 μM
GW4064
E
Relative mRNA expression
Vehicle
0.1 μM
1 μM
10 μM
INT-777
F
PD MSCs
HFD MSCs
Relative mRNA expression
CDCA
G
PD MSC+CDCA
HFD MSC+CDCA
CD90 Wnt2b
PD MSCs
HFD MSCs
Relative Wnt2b expression (MFI)
CDCA

Figure 26. BAs regulate Wnt2b production in colonic MSCs via FXR. (A and B) Relative mRNA expression levels of *Wn2b* were measured in the colonic MSCs treated with CDCA (A) or DCA (B). (C) Immunofluorescence image of nuclei (blue), CD90 (green), and Wnt2b (red) in the colonic MSCs treated with CDCA and relative Wnt2b MFI was calculated based on the control group. Scale bar = 100 μm. (D and E) Relative mRNA expression levels of *Wn2b* were measured in the naïve in vitro colonic MSCs treated with GW4064 (D) or INT-777 (E). (F) Relative mRNA expression levels of *Wn2b* were measured in the colonic MSCs treated with CDCA. (G) Immunofluorescence image of nuclei (blue), CD90 (green), and Wnt2b (red) in the colonic MSCs treated with CDCA and relative Wnt2b MFI was calculated based on the control group. Scale bar = 100 μm. Data are presented as mean ± SD; comparisons were made using the two-tailed t-test, one-way ANOVA, or two-way ANOVA multiple test. *$p < 0.05$, **$p < 0.01$, ***$p < 0.001$. Data were repeated twice in independent experiments.

Discussion

This study demonstrates the dysregulation of colonic stem cells and MSCs in mice fed a HFD through *in vivo* mouse model and *ex vivo* organoids studies. HFD feeding resulted in dysregulation of colonic MSCs, including increased cell numbers, overexpression of Wnt2b, and activation of CAF-like properties. Consistently, HFD-derived colonic MSCs triggered CSC properties and Wnt-related signals. Most importantly, I observed increased BA receptor expression on colonic MSCs, and determined that BAs further stimulate colonic MSC-induced Wnt2b production through the activation of FXR signaling. Overall, my results imply that colonic MSCs play an indispensable role in altering CSCs in HFD-induced tumorigenesis through the BAs-FXR axis.

Earlier studies demonstrated that dietary factors could regulate tumorigenicity of ISCs or intestinal progenitors [30, 72]. The hierarchical CSCs model has been proposed to explain the development of tumorigenicity [73]. As the origin of malignant tumor cells, CSCs are generated by acquiring tumorigenicity through abnormal genetic diversity, epigenetic modification, and signal transduction [73]. In the present study, a HFD resulted in increased CSC properties and Wnt activity in colonic crypts. These results may improve understanding of the mechanisms by which ISCs can become tumor-initiating cells under a HFD. The CD44v isoforms are a critical marker for CRC, and their overexpression is a poor prognostic factor and predictor of metastasis in patients with CRC [64, 74]. Previous studies have been demonstrated an association between CD44v expression and the Wnt signaling pathway in ISCs. For example, CD44v expression was identified in $Lgr5^{+}$ ISCs and contributes to adenoma formation in $Apc^{Min/+}$ mice as a Wnt signal target gene [8, 75]. Furthermore, CD44 supports the activation of Wnt signaling by regulating membrane localization of the Wnt receptor LRP6 [76]. These results imply that CD44 is related to Wnt signal activity, a risk factor for CRC. Given that HFD induced hyper-activation of Wnt signaling in colonic crypts, CD44 overexpression may be an important indicator of intestinal tumorigenesis caused by HFD.

The stem cell niche has duplicity in that it regulates stem cell function and homeostasis while also driving to tumor progression and heterogeneity within the CSC niche [77]. In particular, the formation and maintenance of CSCs have reportedly been regulated extrinsically by the CSC niche [78, 79]. I have demonstrated that overproduction of Wnt2b from HFD-derived MSCs augments the expression of Wnt target genes and CSCs markers in colonic crypts. Other data support these results suggesting that exosomal Wnt ligands from CRC-derived CAFs activate canonical Wnt signaling in cancer cells and subsequently induce CSCs clonogenicity [80]. Previous studies have also highlighted that various CAF-derived factors such as hepatocyte growth factor (HGF) and osteopontin (OPN), can induce Wnt signal activity and promote CSCs clonogenicity [64, 79]. Furthermore, CD44v expression is triggered by factors secreted from CAFs, which subsequently increases the metastatic potential of CRC [64]. Taken together, colonic MSCs may be involved in HFD-induced CRC by contributing to the transformation of ISCs to CSCs and mediating hyper-activation of Wnt signaling.

MSCs are activated into CAFs by signals such as growth factors and chemokines [81]. In this study, RNA-seq data showed that HFD-derived MSCs had CAF-like properties with predominant *CXCR4* and *IL1RL1* expression. The autocrine CXCR4/CXCL12 pathway is known to activate MSCs into tumor-promoting CAFs [67, 81] and subsequently increases survival, migration, and cytokine secretion through PI3K/AKT signaling [82]. Moreover, data have shown that MSCs adjacent to intestinal tumors express IL1RL1 and IL-33, which can induce activation of tumor-promoting MSCs [68]. Transcription factor SOX2-expressing MSCs were presented in the CRC-associated CAFs population, which stimulated tumor progression [69]. Therefore, I speculate that through diverse mechanisms, HFD activates MSCs into CAF-like cells.

Compared with normal MSCs, CAFs are heavily involved in proliferation and metabolism, and increase the production of ECM components and adhesion molecules [83-85]. Given the interaction between the PI3K-Akt pathway and ECM components and cell adhesion molecules [86], the activation of this pathway in HFD-derived MSCs may induce the characterization of CAFs. Furthermore, metabolic changes in HFD-derived MSCs are

consistent with a previous study that showed that PDGF- and TGF-β-induced CAFs undergo metabolic reprogramming [87]. The aerobic glycolysis pathway is subsequently upregulated, causing an increase in lactate production [87]. Moreover, mitochondrial oxidative phosphorylation (OXPHOS) activity is higher in ISCs than Paneth cells, and the OXPHOS demand of ISCs is satisfied by lactate produced by Paneth cells with high glycolytic activity [88]. Therefore, increased glycolytic metabolite in HFD-derived MSCs may affect ISC function. In line with my results, HFD-induced obesity increases differentiation of adipose-derived MSCs into myofibroblasts and production of ECM components, which promote breast tumorigenesis [89]. While my current study focused on colonic MSC-induced Wnt2b overproduction, these CAF-like activities may also contribute to CRC incidence through a HFD. My results suggest that targeting MSCs in the tumor microenvironment or CRC may act as a potential therapeutic strategy.

Gut microbiota is partially formed by and regulates the metabolism of BAs in symbiosis [71, 90]. Cholic acid (CA) feeding has reportedly expanded *Firmicutes* phylum, which subsequently increased the conversion of CA to secondary BAs (deoxycholic acids, DCA) through the 7α-dehydroxylation reaction [59, 91]. Additionally, previous research has shown that various *Bacteroides* strains perform de-conjugation of BAs and 7-keto-DCA/7-dehydro-CDCA biosynthesis, which are important for secondary BA production [92]. In particular, *Bacteroides vulgatus* de-conjugate BAs through BSH activity [71]. Thus, these studies may support the increase of de-conjugated and secondary BAs under conditions of a HFD. Among the BAs metabolized by bacteria, CDCA and DCA were known as cytotoxic BAs that cause DNA damage and subsequently CRC [55, 93, 94]. FXR, a BA-responsive receptor, has a high affinity for CDCA and DCA among the natural ligands [71]. The regeneration of intestinal crypts through inhibition of prostaglandin E2 promoted by the activation of FXR signaling in colonic MSCs has also been reported [55]. My data demonstrate that CDCA and DCA induce Wnt2b production and CAF-like properties from colonic MSCs through activation of FXR signaling. Hence, BA modulation of ISC niche cellular function, such as MSCs, and abnormal function of colonic MSCs by BAs-FXR signaling may act as a risk factor for CRC.

In conclusion, my study demonstrates that aberrant MSCs induced by a HFD drive hyper-proliferation and transition of ISCs to CSCs in the colon. Furthermore, I suggest that BAs hold potential in regulating the function of colonic MSCs. These findings contribute to the improved understanding of the mechanisms by which a HFD may induce CRC, and additionally offer another role for gut microbiota in regulating the function of the ISC niche.

Conclusion

HFD feeding increased the expression of genes related to CSCs and Wnt signaling pathway in the colonic crypts. Along with these results, I demonstrated that HFD caused expansion of colonic subepithelial MSCs and increased production of Wnt2b from MSCs. In addition, increased energy metabolism and CAF-like characteristics were found in colonic MSCs of mice fed with HFD. In the co-culture system of organoid and MSCs, I suggested that colonic MSCs from HFD-fed mice triggered tumorigenic properties in colon organoids. Of note, HFD induced the dysbiosis of gut microbiota, leading to an imbalance in BA metabolism. The levels of deconjugated and secondary BAs increased, which led to activation of the BAs-FXR signaling in MSCs. As a result, BAs-FXR interactions stimulated Wnt2b production in colonic CAF-like MSCs. Taken together, this study suggest that gut microbiota-derived BA metabolism contribute to the HFD-induced CRC development by regulating the function of colonic MSCs through BAs-FXR signal axis.

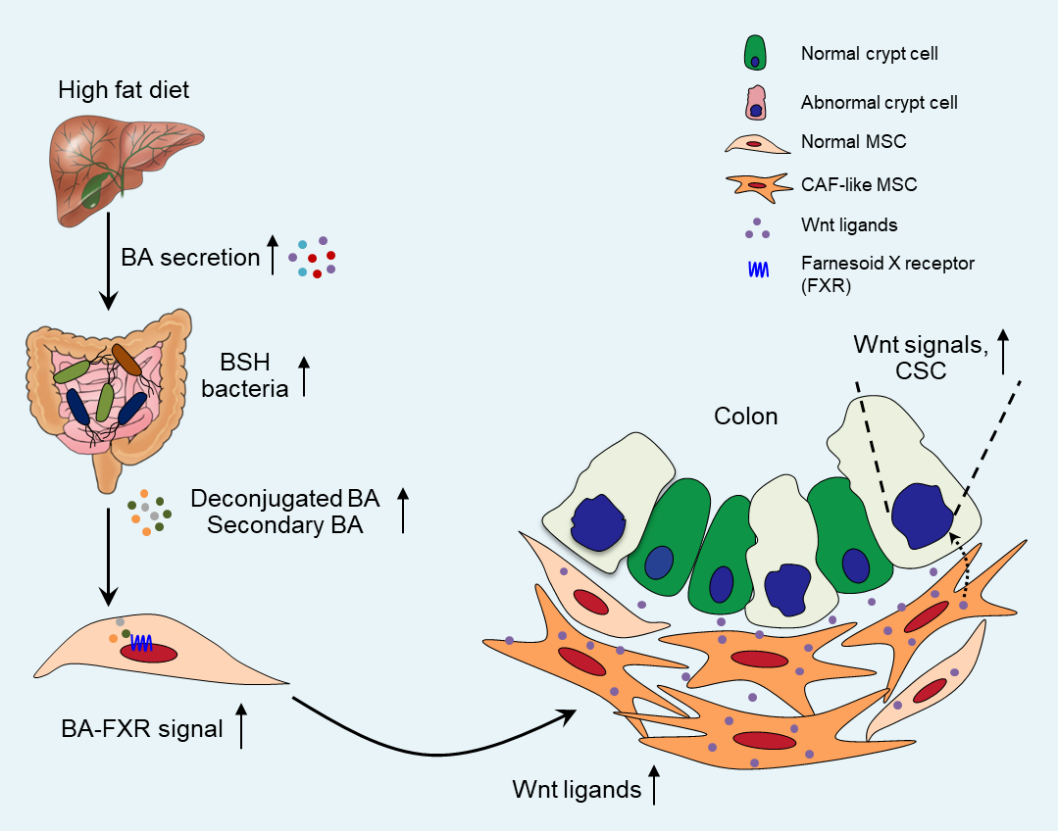

Reference

1. Clevers H. The intestinal crypt, a prototype stem cell compartment. *Cell* 2013;154:274-284.
2. Barker N, van Es JH, Kuipers J, et al. Identification of stem cells in small intestine and colon by marker gene Lgr5. *Nature* 2007;449:1003-1007.
3. de Lau W, Peng WC, Gros P, et al. The R-spondin/Lgr5/Rnf43 module: regulator of Wnt signal strength. *Genes Dev* 2014;28:305-316.
4. Barriga FM, Montagni E, Mana M, et al. Mex3a marks a slowly dividing subpopulation of $Lgr5^{+}$ intestinal stem cells. *Cell Stem Cell* 2017;20:801-816 e7.
5. Barker N, Ridgway RA, van Es JH, et al. Crypt stem cells as the cells-of- origin of intestinal cancer. *Nature* 2009;457:608-611.
6. de Sousa e Melo F, Kurtova AV, Harnoss JM, et al. A distinct role for $Lgr5^{+}$ stem cells in primary and metastatic colon cancer. *Nature* 2017;543:676-680
7. Walcher L, Kistenmacher A-K, Suo H, et al. Cancer stem cells—origins and biomarkers: perspectives for targeted personalized therapies. *Frontiers in Immunology* 2020;11.
8. Zeilstra J, Joosten SP, Dokter M, et al. Deletion of the Wnt target and cancer stem cell marker CD44 in $Apc^{Min/+}$ mice attenuates intestinal tumorigenesis. *Cancer Res* 2008;68:3655-3661.
9. Merlos-Suárez A, Barriga Francisco M, Jung P, et al. The intestinal stem cell signature identifies colorectal cancer stem cells and predicts disease relapse. *Cell Stem Cell* 2011;8:511-524.
10. Sato T, van Es JH, Snippert HJ, et al. Paneth cells constitute the niche for Lgr5 stem cells in intestinal crypts. *Nature* 2010;469:415-418.
11. Farin HF, Van Es JH, Clevers H. Redundant sources of Wnt regulate intestinal stem cells and promote formation of paneth cells. *Gastroenterology* 2012;143:1518-1529 e7.
12. Kabiri Z, Greicius G, Madan B, et al. Stroma provides an intestinal stem cell niche in the absence of epithelial Wnts. *Development* 2014;141:2206-2215.

13. Valenta T, Degirmenci B, Moor AE, et al. Wnt ligands secreted by subepithelial mesenchymal cells are essential for the survival of intestinal stem cells and gut homeostasis. *Cell Rep* 2016;15:911-918.

14. Sasaki N, Sachs N, Wiebrands K, et al. Reg4^{+} deep crypt secretory cells function as epithelial niche for Lgr5^{+} stem cells in colon. *Proc Natl Acad Sci USA* 2016;113:E5399-E5407.

15. Sailaja BS, He XC, Li L. The regulatory niche of intestinal stem cells. *J Physiol* 2016;594:4827-4836.

16. Shoshkes-Carmel M, Wang YJ, Wangensteen KJ, et al. Subepithelial telocytes are an important source of Wnts that supports intestinal crypts. *Nature* 2018;557:242-246.

17. Gong W, Guo M, Han Z, et al. Mesenchymal stem cells stimulate intestinal stem cells to repair radiation-induced intestinal injury. *Cell Death Dis* 2016;7:e2387.

18. Stzepourginski I, Nigro G, Jacob J-M, et al. CD34^{+} mesenchymal cells are a major component of the intestinal stem cells niche at homeostasis and after injury. *Proc Natl Acad Sci USA* 2017;114:E506-E513.

19. Degirmenci B, Valenta T, Dimitrieva S, et al. GLI1-expressing mesenchymal cells form the essential Wnt-secreting niche for colon stem cells. *Nature* 2018;558:449-453.

20. Koliaraki V, Pallangyo CK, Greten FR, et al. Mesenchymal cells in colon cancer. *Gastroenterology* 2017;152:964-979.

21. Clevers H, Loh KM, Nusse R. Stem cell signaling. an integral program for tissue renewal and regeneration: Wnt signaling and stem cell control. *Science* 2014;346:1248012.

22. Anastas JN, Moon RT. Wnt signalling pathways as therapeutic targets in cancer. *Nat Rev Cancer* 2013;13:11-26.

23. Fu L, Zhang C, Zhang L-Y, et al. Wnt2 secreted by tumour fibroblasts promotes tumour progression in oesophageal cancer by activation of the Wnt/β-catenin signalling pathway. *Gut* 2011;60:1635-1643.

24. Huels DJ, Bruens L, Hodder MC, et al. Wnt ligands influence tumour initiation by controlling the number of intestinal stem cells. *Nat Commun* 2018;9:1132.

25. Igarashi M, Guarente L. mTORC1 and SIRT1 cooperate to foster expansion of gut adult stem cells during calorie restriction. *Cell* 2016;166:436-450.
26. Mihaylova MM, Sabatini DM, Yilmaz OH. Dietary and metabolic control of stem cell function in physiology and cancer. *Cell Stem Cell* 2014;14:292-305.
27. Yilmaz Ö H, Katajisto P, Lamming DW, et al. mTORC1 in the paneth cell niche couples intestinal stem-cell function to calorie intake. *Nature* 2012;486:490-495.
28. Cheng CW, Biton M, Haber AL, et al. Ketone body signaling mediates intestinal stem cell homeostasis and adaptation to diet. *Cell* 2019;178:1115-1131.
29. Deng H, Gerencser AA, Jasper H. Signal integration by Ca^{2+} regulates intestinal stem-cell activity. *Nature* 2015;528:212-217.
30. Beyaz S, Mana MD, Roper J, et al. High-fat diet enhances stemness and tumorigenicity of intestinal progenitors. *Nature* 2016;531:53-58.
31. Sender R, Fuchs S, Milo R. Revised estimates for the number of human and bacteria cells in the body. *PLoS Biol* 2016;14:e1002533.
32. Walter J, Ley R. The human gut microbiome: ecology and recent evolutionary changes. *Annu Rev Microbio* 2011;65:411-429.
33. Zmora N, Suez J, Elinav E. You are what you eat: diet, health and the gut microbiota. *Nat Rev Gastroenterol Hepatol* 2019;16:35-56.
34. DeGruttola AK, Low D, Mizoguchi A, et al. Current understanding of dysbiosis in disease in human and animal models. *Inflamm Bowel Dis* 2016;22:1137-1150.
35. Hildebrandt MA, Hoffmann C, Sherrill-Mix SA, et al. High-fat diet determines the composition of the murine gut microbiome independently of obesity. *Gastroenterology* 2009;137:1716-24.e1-2.
36. Kim K-A, Gu W, Lee I-A, et al. High fat diet-induced gut microbiota exacerbates inflammation and obesity in mice via the TLR4 signaling pathway. *PLoS One* 2012;7:e47713.
37. Araújo JR, Tomas J, Brenner C, et al. Impact of high-fat diet on the intestinal microbiota and small intestinal physiology before and after the onset of obesity. *Biochimie* 2017;141:97-106.

38. Ding S, Chi MM, Scull BP, et al. High-fat diet: bacteria interactions promote intestinal inflammation which precedes and correlates with obesity and insulin resistance in mouse. *PLoS One* 2010;5:e12191.

39. Yoo W, Zieba JK, Foegeding NJ, et al. High-fat diet–induced colonocyte dysfunction escalates microbiota-derived trimethylamine N-oxide. *Science* 2021;373:813-818.

40. Gulhane M, Murray L, Lourie R, et al. High fat diets induce colonic epithelial cell stress and inflammation that is reversed by IL-22. *Sci Rep* 2016;6:28990.

41. Manichanh C, Borruel N, Casellas F, et al. The gut microbiota in IBD. *Nat Rev Gastroenterol Hepatol* 2012;9:599-608.

42. Sun J, Qiao Y, Qi C, et al. High-fat-diet–induced obesity is associated with decreased antiinflammatory Lactobacillus reuteri sensitive to oxidative stress in mouse Peyer's patches. *Nutrition* 2016;32:265-272.

43. Yi W, Fenglei W, Jihong Y, et al. Effects of dietary fat on gut microbiota and faecal metabolites, and their relationship with cardiometabolic risk factors: a 6-month randomised controlled-feeding trial. *Gut* 2019;68:1417-1429.

44. Furusawa Y, Obata Y, Fukuda S, et al. Commensal microbe-derived butyrate induces the differentiation of colonic regulatory T cells. *Nature* 2013;504:446-450.

45. He Y, Fu L, Li Y, et al. Gut microbial metabolites facilitate anticancer therapy efficacy by modulating cytotoxic $CD8^+$ T cell immunity. *Cell Met* 2021;33:988-1000.

46. Dalby MJ, Ross AW, Walker AW, et al. Dietary uncoupling of gut microbiota and energy harvesting from obesity and glucose tolerance in mice. *Cell Rep* 2017;21:1521-1533.

47. Schulz MD, Atay Ç, Heringer J, et al. High-fat-diet-mediated dysbiosis promotes intestinal carcinogenesis independently of obesity. *Nature* 2014;514:508-512.

48. Beyaz S, Chung C, Mou H, et al. Dietary suppression of MHC class II expression in intestinal epithelial cells enhances intestinal tumorigenesis. *Cell Stem Cell* 2021;28:1922-1935.e5.

49. Chiang JY. Bile acid metabolism and signaling. *Compr Physiol* 2013;3:1191-212.

50. Sinal CJ, Tohkin M, Miyata M, et al. Targeted disruption of the nuclear receptor FXR/BAR impairs bile acid and lipid homeostasis. *Cell* 2000;102:731-744.

51. de Aguiar Vallim Thomas Q, Tarling Elizabeth J, Edwards Peter A. Pleiotropic roles of bile acids in metabolism. *Cell Metab* 2013;17:657-669.

52. Wahlström A, Sayin SI, Marschall HU, et al. Intestinal crosstalk between bile acids and microbiota and its impact on host metabolism. *Cell Metab* 2016;24:41-50.

53. Sayin SI, Wahlström A, Felin J, et al. Gut microbiota regulates bile acid metabolism by reducing the levels of tauro-beta-muricholic acid, a naturally occurring FXR antagonist. *Cell Metab* 2013;17:225-235.

54. Duboc H, Rajca S, Rainteau D, et al. Connecting dysbiosis, bile-acid dysmetabolism and gut inflammation in inflammatory bowel diseases. *Gut* 2013;62:531-539.

55. Jain U, Lai CW, Xiong S, et al. Temporal regulation of the bacterial metabolite deoxycholate during colonic repair is critical for crypt regeneration. *Cell Host Microbe* 2018;24:353-363.

56. Fu T, Coulter S, Yoshihara E, et al. FXR regulates intestinal cancer stem cell proliferation. *Cell* 2019;176:1098-1112.

57. Sorrentino G, Perino A, Yildiz E, et al. Bile acids signal via TGR5 to activate intestinal stem cells and epithelial regeneration. *Gastroenterology* 2020;159:956-968.e8.

58. Dieleman LA, Palmen MJ, Akol H, et al. Chronic experimental colitis induced by dextran sulphate sodium (DSS) is characterized by Th1 and Th2 cytokines. *Clin Exp Immunol* 1998;114:385-391.

59. Islam KB, Fukiya S, Hagio M, et al. Bile acid is a host factor that regulates the composition of the cecal microbiota in rats. *Gastroenterology* 2011;141:1773-1781.

60. Sato T, Vries RG, Snippert HJ, et al. Single Lgr5 stem cells build crypt-villus structures in vitro without a mesenchymal niche. *Nature* 2009;459:262-265.

61. Koliaraki V, Kollias G. Isolation of intestinal mesenchymal cells from adult mice. *Bio-protocol* 2016;6:e1940.

62. Segata N, Izard J, Waldron L, et al. Metagenomic biomarker discovery and explanation. *Genome Biol* 2011;12:R60.

63. Sonnenburg ED, Smits SA, Tikhonov M, et al. Diet-induced extinctions in the gut microbiota compound over generations. *Nature* 2016;529:212-215.

64. Todaro M, Gaggianesi M, Catalano V, et al. CD44v6 is a marker of constitutive and reprogrammed cancer stem cells driving colon cancer metastasis. *Cell Stem Cell* 2014;14:342-356.

65. Du L, Wang H, He L, et al. CD44 is of functional importance for colorectal cancer stem cells. *Clin Cancer Res* 2008;14:6751-6760.

66. Karpus ON, Westendorp BF, Vermeulen JLM, et al. Colonic CD90+ crypt fibroblasts secrete semaphorins to support epithelial growth. *Cell Rep* 2019;26:3698-3708.

67. Toullec A, Gerald D, Despouy G, et al. Oxidative stress promotes myofibroblast differentiation and tumour spreading. *EMBO Mol Med* 2010;2:211-230.

68. Maywald RL, Doerner SK, Pastorelli L, et al. IL-33 activates tumor stroma to promote intestinal polyposis. *Proc Natl Acad Sci USA* 2015;112:E2487-2496.

69. Kasashima H, Duran A, Martinez-Ordonez A, et al. Stromal SOX2 upregulation promotes tumorigenesis through the generation of a SFRP1/2-expressing cancer-associated fibroblast population. *Dev Cell* 2021;56:95-110 e10.

70. Yoshimoto S, Loo TM, Atarashi K, et al. Obesity-induced gut microbial metabolite promotes liver cancer through senescence secretome. *Nature* 2013;499:97-101.

71. Fiorucci S, Distrutti E. Bile Acid-Activated Receptors, Intestinal microbiota, and the treatment of metabolic disorders. *Trends Mol Med* 2015;21:702-714.

72. Kim E, Davidson LA, Zoh RS, et al. Rapidly cycling Lgr5^{+} stem cells are exquisitely sensitive to extrinsic dietary factors that modulate colon cancer risk. *Cell Death Dis* 2016;7:e2460.

73. Medema JP. Cancer stem cells: the challenges ahead. *Nat Cell Biol* 2013;15:338-344.

74. Wang Z, Tang Y, Xie L, et al. The prognostic and clinical value of CD44 in colorectal cancer: a meta-analysis. *Front Oncol* 2019;9:309.

75. Zeilstra J, Joosten SP, van Andel H, et al. Stem cell CD44v isoforms promote intestinal cancer formation in Apc(min) mice downstream of Wnt signaling. *Oncogene* 2014;33:665-670.

76. Schmitt M, Metzger M, Gradl D, et al. CD44 functions in Wnt signaling by regulating LRP6 localization and activation. *Cell Death Differ* 2015;22:677-689.

77. Plaks V, Kong N, Werb Z. The cancer stem cell niche: how essential is the niche in regulating stemness of tumor cells? *Cell Stem Cell* 2015;16:225-238.

78. Charles N, Ozawa T, Squatrito M, et al. Perivascular nitric oxide activates notch signaling and promotes stem-like character in PDGF-induced glioma cells. *Cell Stem Cell* 2010;6:141-152.

79. Vermeulen L, De Sousa E Melo F, van der Heijden M, et al. Wnt activity defines colon cancer stem cells and is regulated by the microenvironment. *Nat Cell Biol* 2010;12:468-476.

80. Hu YB, Yan C, Mu L, et al. Exosomal Wnt-induced dedifferentiation of colorectal cancer cells contributes to chemotherapy resistance. *Oncogene* 2019;38:1951-1965.

81. Kojima Y, Acar A, Eaton EN, et al. Autocrine TGF-β and stromal cell-derived factor-1 (SDF-1) signaling drives the evolution of tumor-promoting mammary stromal myofibroblasts. *Proc Natl Acad Sci USA* 2010;107:20009-200014.

82. Liu X, Duan B, Cheng Z, et al. SDF-1/CXCR4 axis modulates bone marrow mesenchymal stem cell apoptosis, migration and cytokine secretion. *Protein Cell* 2011;2:845-854.

83. Becker LM, O'Connell JT, Vo AP, et al. Epigenetic reprogramming of cancer-associated fibroblasts deregulates glucose metabolism and facilitates progression of breast cancer. *Cell Rep* 2020;31:107701.

84. Labernadie A, Kato T, Brugues A, et al. A mechanically active heterotypic E-cadherin/N-cadherin adhesion enables fibroblasts to drive cancer cell invasion. *Nat Cell Biol* 2017;19:224-237.

85. Erdogan B, Ao M, White LM, et al. Cancer-associated fibroblasts promote directional cancer cell migration by aligning fibronectin. *J Cell Biol* 2017;216:3799-3816.

86. Reif S, Lang A, Lindquist JN, et al. The role of focal adhesion kinase-phosphatidylinositol 3-kinase-akt signaling in hepatic stellate cell proliferation and type I collagen expression. *J Biol Chem* 2003;278:8083-8090.

87. Zhang D, Wang Y, Shi Z, et al. Metabolic reprogramming of cancer-associated fibroblasts by IDH3α downregulation. *Cell Rep* 2015;10:1335-1348.

88. Rodríguez-Colman MJ, Schewe M, Meerlo M, et al. Interplay between metabolic identities in the intestinal crypt supports stem cell function. Nature 2017;543:424-427.

89. Seo BR, Bhardwaj P, Choi S, et al. Obesity-dependent changes in interstitial ECM mechanics promote breast tumorigenesis. Sci Transl Med 2015;7:301ra130.

90. Zheng X, Huang F, Zhao A, et al. Bile acid is a significant host factor shaping the gut microbiome of diet-induced obese mice. BMC Biol 2017;15:120.

91. Ridlon JM, Alves JM, Hylemon PB, et al. Cirrhosis, bile acids and gut microbiota: unraveling a complex relationship. Gut Microbes 2013;4:382-387.

92. Heinken A, Ravcheev DA, Baldini F, et al. Systematic assessment of secondary bile acid metabolism in gut microbes reveals distinct metabolic capabilities in inflammatory bowel disease. Microbiome 2019;7:75.

93. Powolny A, Xu J, Loo G. Deoxycholate induces DNA damage and apoptosis in human colon epithelial cells expressing either mutant or wild-type p53. Int J Biochem Cell Biol 2001;33:193-203.

94. Yui S, Kanamoto R, Saeki T. Biphasic regulation of cell death and survival by hydrophobic bile acids in HCT116 cells. Nutr Cancer 2009;61:374-380.

국문 요약

다양한 식이 요소들은 장 줄기세포의 증식과 유지뿐만 아니라 장 줄기세포의 종양 형성을 조절하는 것으로 알려져 있다. 이전의 연구들에서는 고지방식이가 장 줄기세포의 수를 증가시키고 대장암의 발생과 전이를 더욱 촉진한다는 것이 입증되었다. 특히 장 줄기세포의 주변 세포들이 대장암의 발병에서도 중요한 역할을 하는 것으로 알려져 있지만, 이러한 주변 세포들에 대한 고지방 식이의 영향은 잘 알려져 있지 않다. 따라서 줄기세포의 주변 세포들에 대한 영향을 이해하는 것이 고지방식이에 의한 대장암 유도 기전을 규명하는 데 있어서 중요한 기반 중 하나가 될 것이다. 본 연구에서는 고지방식이가 대장 선와에서 증식하는 $Ki67^+$ 세포 수를 증가시켰음을 확인하였다. 또한, 종양줄기세포 마커들의 발현과 Wnt 신호가 고지방식이를 먹인 마우스의 대장 선와 및 오가노이드에서 상당히 증가했음을 발견하였다. 이와 유사하게, 고지방식이는 대장의 상피층 아래 섬유아세포의 확장과 섬유아세포로부터 Wnt2b 분비를 자극하였다. 또한, 고지방식이를 먹인 마우스의 대장 섬유아세포에서 에너지 대사가 증가하며 종양과 관련된 섬유아세포와 유사한 특성이 관찰되었다. 특히, 대장 섬유아세포와 오가노이드의 공동 배양 시스템에서 고지방식이를 먹인 마우스에서 유래한 대장 섬유아세포는 대장 오가노이드의 증식 및 종양줄기세포 마커들의 발현을 유도하였다. 이는 식이 요소가 줄기세포의 주변 세포들의 기능을 조절할 수 있고 섬유아세포가 고지방식이로 인한 대장암 발병에 중요한 역할을 할 수 있음을 시사한다. 장내 미생물 분석 결과, 대조 식이를 먹인 마우스에 비해 고지방식이를 먹인 마우스의 분변에서 장내 세균 총의 다양성이 감소하고 분포도가 변해있음을 발견하였다. 특히, 고지방식이를 먹인 마우스의 장내 세균 총에서 담즙산 대사에 관여하는 세균의 분포가 증가함에 따라 1 차 및 2 차 담즙산 농도가 유의적으로 증가하였다. 담즙산에 의한 FXR 신호의 활성화는 대장 섬유아세포에서 Wnt2b 생산을 자극한다는 것이 입증되었다. 종합해보면, 장내 미생물에 의한 담즙산 대사는 FXR 신호 전달을 통해 대장 섬유아세포의 기능을 조절함으로써 고지방식이에 따른 대장암 발병에 기여할 수 있음을 제시하였다.

중심단어: 고지방식이, 종양줄기세포, 섬유아세포, Wnt2b, 담즙산, FXR